Manuel K. Strauss, BSc

Ciprofloxacin - a Computational Study of UV Spectra and Protonation Equilibria

MASTERARBEIT

zur Erlangung des akademischen Grades

Master of Science

Masterstudium Chemie

eingereicht an der

Technischen Universität Graz

Betreuerin

Ao.Univ.-Prof. Dipl.-Ing. Dr.techn. Anne-Marie Kelterer

Institut für Physikalische und Theoretische Chemie

Graz, Juli und 2017

EIDESSTATTLICHE ERKLÄRUNG

Ich erkläre an Eides statt, dass ich die vorliegende Arbeit selbstständig verfasst, andere als die angegebenen Quellen/Hilfsmittel nicht benutzt, und die den benutzten Quellen wörtlich und inhaltlich entnommenen Stellen als solche kenntlich gemacht habe. Das in TUGRAZonline hochgeladene Textdokument ist mit der vorliegenden Masterarbeit identisch.

Datum

Unterschrift

Abstract

This thesis is a computational study about ciprofloxacin (CIP), a comercially important antibiotic. This fluoroquinolone possesses various tautomeric forms, of which we predict the UV absorptions and acid dissociation constants (pK_a). Experimental UV-Vis spectra and macroscopic pK_a of pharmaceutical drugs usually represent a mixture of various protonation states and/or tautomers. The theoretical prediction of these constants and UV peaks supports the experimentalist in the attribution of these parameters to the respective species. The aim of this work is to find the best combination of DFT method, basis set and continuum solvation model for this task. For this purpose, 2-naphthol and 4-nitrophenol serve as benchmark molecules. CAM-B3LYP/6-311+G(d)/SMD was found to be the most reliable combination regarding the computation of acid dissociation constants, whereas for UV spectra APFD/def2-TZVP/SMD performed best. These methods were applied to predict several properties of ciprofloxacin, including tautomeric constants, acid dissociation constants, electronic transitions and the protonation pathway. Acid dissociation constants of the cationic and the neutral form of ciprofloxacin deviated by less than 1.5 pK_a units of the experimental values. The experimental UV spectra of ciprofloxacin were successfully predicted to primarily consist of the anion in a basic (pH 11), the zwitterion in a neutral and the cation in an acidic (pH 2) aqueous medium. These results as well as the computed protonation pathway are in line with the experimental data found in literature.

Kurzfassung

Diese Arbeit beinhaltet eine theoretische Studie über Ciprofloxacin, einem kommerziell wichtigen Antibiotikum. Experimentelle UV-Vis Spektren und makroskopische Säurekonstanten von Pharmazeutika repräsentieren häufig eine Mischung aus verschiedenen Protonierungszuständen und/oder Tautomeren. Die theoretische Vorhersage von elektronischen Übergängen und pK_a untertsützt Experimentalisten bei der eindeutigen Zuordnung dieser Parameter. Das Ziel dieser Arbeit ist es, die beste Kombination aus DFT-Methode, Basissatz und Lösungsmittelmodell für diese Aufgabe zu finden. Zu diesem Zweck wurden 2-Naphthol und 4-Nitrophenol als Benchmark-Moleküle verwendet. Es stellte sich heraus, dass CAM-B3LYP/6-311+G(d)/SMD am geeignetsten zur Berechnung von Säurekonstanten ist, wohingegen APFD/def2-TZVP/SMD die besten UV-Spektren liefert. Diese Methoden wurden zur Berechnung der Eigenschaften von Ciprofloxacin verwendet, darunter Tautomeriekonstanten, Säurekonstanten, elektronische Übergänge und den Protonierungspfad. Säurekonstanten der neutralen und kationischen From von Ciprofloxacin wichen weniger als 1.5 pK_a Einheiten vom Experiment ab. Es wurde berechnet, dass die experimentellen Spektren vorwiegend aus dem Anion im basischen (pH 11), dem Zwitterion im neutralen und dem Kation im sauren (pH 2) wässrigen Medium bestehen. Diese Resultate sowie der berechnete Protonierungspfad stimmen gut mit den experimentellen Literaturdaten überein.

Acknowledgements

I am grateful to Univ.-Prof. Mag.rer.nat. Dr.phil. Georg Gescheidt-Demner, the head of the Institute of Physical and Theoretical Chemistry for providing the equipment required for this work.

I owe my deepest gratitude to my supervisor Ao.Univ.-Prof. Dipl.-Ing. Dr.techn. Anne-Marie Kelterer for the opportunity to write this thesis and all the patience and support she gave me along the way.

My gratitude also belongs to our cooperator in Argentina, Milagros Montemurro, for providing the experimental spectra of ciprofloxacin and the permission to publish them.

My special thanks go out to Magdalena Traber, MSc., for both her advice and proofreading.

Finally, I want to thank my family and my friends for their support during my studies.

Contents

Abstract iii

Kurzfassung iv

Acknowledgements v

Introduction 1

1 Theoretical Methods 4
- 1.1 DFT Methods . . . 4
  - 1.1.1 APF-D . . . 5
  - 1.1.2 BMK . . . 6
  - 1.1.3 CAM-B3LYP . . . 8
  - 1.1.4 M06-2X . . . 9
  - 1.1.5 PBE0 . . . 10
- 1.2 Basis Sets . . . 11
  - 1.2.1 Pople Basis Sets . . . 12
  - 1.2.2 Correlation-consistent Basis Sets . . . 13
  - 1.2.3 Karlsruhe Basis Sets . . . 14
- 1.3 Employed Basis Sets . . . 15
- 1.4 Continuum Solvation Models . . . 15
  - 1.4.1 Polarizable Continuum Model . . . 17
  - 1.4.2 Conductor-like Polarizable Continuum Model . . . 18
  - 1.4.3 Solvation Model based on Density . . . 19
- 1.5 Computational Details . . . 20

2 Nomenclature 22

3 Workflow 25

4 Conformations of Ciprofloxacin 28

5 Calculation of the pK_a **32**
5.1 General . . . 32
5.2 Thermodynamic Cycles . . . 33
5.2.1 The Born-Haber Cycle . . . 34
5.2.2 Protocols for pK_a Calculation . . . 35
5.3 Calculation of pK_a^*: the Förster cycle . . . 38

6 Results and Discussion **40**
6.1 Acid Dissociation Constants . . . 40
6.1.1 Benchmark Calculations . . . 40
6.1.2 pK_a Calculation of Ciprofloxacin . . . 45
6.2 UV-Vis Results . . . 53
6.2.1 Experimental Spectra . . . 53
6.2.2 Calculated Absorption Spectra of 2N and CIP . . . 54
6.2.3 Impact of Conformation on Spectra . . . 56
6.2.4 Absorption Band Deviations among DFT Methods . . . 57
6.3 MO Interpretation for CIP . . . 60
6.4 HOMO-LUMO Energies . . . 67

7 Conclusion **69**

8 Appendix **72**

Bibliography **78**

List of Figures

0.1 Tested compounds: 2N, 4NP and CIP 2

2.1 Nomenclature of ciprofloxacin in this work 22

3.1 Depiction of the workflow 25
3.2 Preferred uncharged conformers of CIP 26

4.1 Tested conformations of uncharged CIP 29

5.1 Thermodynamic cycle 34
5.2 The protolytic Förster cycle 38

6.1 2N: ground and excited state pK_a 41
6.2 Calculated protonation pathway of CIP 48
6.3 Protonation pathways in literature 49
6.4 Experimental UV spectra of CIP 53
6.5 Comparison of methods: UV spectra of neutral and zwitterionic CIP 54
6.6 Calculated UV spectra of CIP's protonation states 55
6.7 Influence of the 0/1 conformation on the UV spectrum 56
6.8 1^{st} major transition: MOs of the anion, neutral and cation 62
6.9 1^{st} major transition: MOs of the zwitterion and the dication 63
6.10 2^{nd} major transition: MOs of all forms except the dication 64
6.11 3^{rd} major transition: MOs of the anion, neutral and cation 65
6.12 3^{rd} major transition: MOs of the zwitterion and the dication 66
6.13 HOMO and LUMO energies of CIP 67

8.1 MOs of CIP^- 73
8.2 MOs of the neutral CIPH 74
8.3 MOs of the zwitterionic CIPH 75
8.4 MOs of $CIPH_2^+$ 76
8.5 MOs of $CIPH_3^{2+}$ 77

Introduction

Computational chemistry on pharmaceutical compounds can help solving their structure and reaction mechanisms as well as describe their properties. One interesting class of compounds are fluoroquinolones. They are both widely used and commercially important, as they are able to cure a variety of infections.

Ciprofloxacin (CIP) is a class II quinolone and well known as a pharmaceutical drug with antibiotic action. It possesses various protonation sites and can act as photoacid with its various tautomeric forms. Accordingly, experimentally obtained macroscopic acid dissociation constants (pK_a) and UV spectra of ciprofloxacin stem from a mixture of several protonation states and/or conformers.

The main purpose of this thesis is the computational study of the tautomers of CIP and their effect on the spectral properties. The presence of certain tautomeric forms at a particular pH value can be clarified by extracting protonation equilibria - which are ambiguous in literature - from ground and excited state data.

This thesis aims to help experimentalists with the assignment of their data to specific forms of fluoroquinolones by finding a reliable and cost-efficient computational method to perform these calculations.

The photostability of drugs is one of the major factors concerning their degradation. Many pharmaceuticals possess big π-systems and are photoacids - substances, which abstract a proton upon photoexcitation. The excited state pK_a can be calculated from the shift of the corresponding absorption/emission peak between the acid and its conjugated base. While this can be done experimentally, attributing the peaks to specific protonation states and tautomers might pose a problem. Therefore, the second goal of this thesis is the to find a combination of method and basis set which accurately predicts electronic transitions and the resulting UV-Vis spectra. To achieve these goals, several important aspects have to be considered:

1.) Most pharmaceuticals are relatively big molecules
Therefore, using large basis sets would require too many resources, as would high-level methods such as Hartree-Fock and post-Hartree-Fock. Force field methods may be cheap, but are certainly too inaccurate for the task. The Density Functional

method has been found as a good compromise between effectiveness and accuracy, therefore methods employing this theory (DFT) were chosen for testing.

2.) Many drugs contain several moieties which can be protonated/deprotonated
As many drugs possess states with multiple positive and/or negative charges, gas-phase calculations do not seem like a reliable approach. Additionally, the protonation/deprotonation of drugs occurs in aqueous solution, thus they also have to be calculated in solution. Explicit solvation would be too costly, therefore the continuum solvent models PCM, CPCM and SMD were chosen for testing.

3.) Many drugs possess several possible conformations
This is a very important aspect regarding the validity of pK_a calculations. As the energies calculated in a continuum solvent are generally viewed as unphysical, thermodynamic cycles are employed. These cycles use both gas and condensed phase optimized geometries and operate on the assumption that both are roughly the same. However, it is not unusual for a conformation to be favoured in gas phase, but not in solution - thus the calculations might converge towards different geometries, potentially rendering the approach invalid. Alternatively, pK_a values can be calculated using just the solvent energies, which generally yields reliable results. Tests will therefore include both approaches.

Three molecules have been chosen as the objects of the calculations (see Figure 0.1):

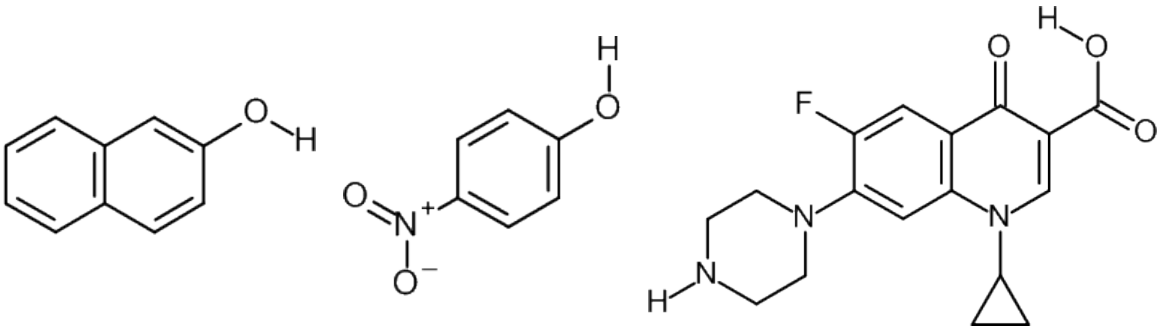

Figure 0.1: Compounds used in this work: 2-naphtol (left), 4-nitrophenol (center) and ciprofloxacin (right).

a) 2-naphthol (2N), a benchmark molecule with both experimentally and theoretically well known ground and excited state properties
b) 4-nitrophenol (4NP), another benchmark molecule with a charge separation at the NO_2 moiety and known pK_a

c) ciprofloxacin (CIP), a fluoroquinolone which is a commercially important antibiotic and the main molecule in this thesis

2N and 4NP were used as benchmark molecules to find the best combination of method/basis set/solvation model. The selected method has then been used to compute several properties of CIP, such as the protonation equilibria and UV spectra, whereby most of them possess all challenging aspects mentioned before.

Chapter 1 introduces the reader to the methods, basis sets and the solvation models used in this work. Chapter 2 describes the nomenclature of ciprofloxacin and Chapter 3 explains the workflow of this thesis. Chapter 4 highlights the influence of the conformation on the energy by comparing the energies of conformers. The theoretical background and the results regarding the calculation of the acid dissociation constant are handled in Chapter 5 and the beginning of Chapter 6, respectively. The rest of Chapter 6 is concerned with the calculations of the electronic transitions and orbitals. The conclusions regarding this work are drawn in Chapter 7, followed by the Appendix (Chapter 8) and the Bibliography.

1 Theoretical Methods

This chapter provides the background information for all methods, basis sets and continuum solvation models employed in the calculations, as well as details concerning those calculations.

1.1 DFT Methods

This section roughly outlines the density functional theory (DFT) methods used in this work. The background information has been taken from Cramer's 'Essentials of Computational Chemistry: Theories and Models' [1]. Density functional theory is a quantum mechanical modeling method. Atom and molecule properties as well as energies are calculated based on the spatial distribution of electron density, which is a physical observable - unlike the wave function used in ab initio calculations. The approach was legitimized by the two Hohenberg–Kohn theorems: one which proves that the ground state properties depend on the electron density, and one which defines a functional that possesses an energetical minimum at the correct ground state. Kohn and Sham simplified the calculations by assuming that the electrons are non-interacting but the ground state density is still the same as in the real system. This way, the Hamiltonian is equal to the sum of all one-electron operators, or Kohn-Sham operators, and the interaction between electrons is defined by the exchange and the correlation interaction.
Several DFT methods have been tested in this thesis: PBE0, M06-2X, CAM-B3LYP and BMK have been chosen for their perfomance in pK_a calculation as reported by Jaquemin and coworkers. [2] Additionally, the same four functionals are quite accurate regarding the calculation of absorption spectra, as is another functional called APFD.[3][4] These functionals possess the following amount of HF exchange:

- APFD - 23%
- BMK - 42%
- CAM-B3LYP - 19% at short range, 65% at long range
- M06-2X - 54%
- PBE0 - 25%

1.1.1 APF-D

The information about this method has been gained from the work of Austin et al.[5] APF-D is a combination of a density functional ('APF') and an empirical dispersion add-on ('-D') to achieve a proper behavior for long-range interactions. APF is an acronym of its creators surnames - A. Austin, G. A. Peterson and M. J. Frisch.

A Spherical Atom Model (SAM), which is an atom-atom pairwise potential function, is used for the add-on. It describes the dispersion force resulting from the interaction of two spherical shells of polarizable medium.

SAM is based on two non-exact but cost-efficient assumptions:

- the intermolecular dispersion interaction equals the sum of the spherically symmetric atomic interactions of each atom pair
- transfer of atomic parameters is possible

APF-Functional
The APF functional is a dispersionless linear combination of functionals, consisting to 41.1% of B3PW91 and 58.9% of PBE0. These two functionals have been chosen due to the cancellation of spurious long-range interactions while remaining cost-efficient. Its calculations are based on nine parameters and two computed atomic properties: the effective atomic polarizability and the ionization potential. Futhermore, it possesses a Hartree-Fock exchange of 23%.

SAM for Dispersion
$V(R_{AB})$, the interatomic potential, is described as follows:

$$V(R_{AB}) \approx \frac{C_{6,AB}}{R_{AB}^6}\left[1 + 3\left(\frac{r_{s,A} + r_{s,B}}{R_{AB}}\right)^2 + 6\left(\frac{r_{s,A} + r_{s,B}}{R_{AB}}\right)^4 + ...\right] \tag{1.1}$$

- R_{AB}: distance between the atoms A and B
- $C_{6,AB}$: coefficient for the -6^{th} power of the distance between the atoms.
- $r_{s,A/B}$: radius of the sphere of A/B

The formula is constructed like a Taylor series to provide the contributions from R^{-8} and R^{-10}, while avoiding the need to add the coefficients $C_{8,AB}$ and $C_{10,AB}$.

For a proper description of short-range interactions equation 1.1 has to be combined with a damping function. For this purpose, the damping radius $R_{d,AB}$ is used.

$$f(R_{AB}) = \begin{cases} 0 & R_{AB} \leq R_{d,AB} \\ \left[1 - \left(1 + 2 * \frac{R_{AB} - R_{d,AB}}{R_{d,AB}}\right) * e^{-4\left(\frac{R_{AB} - R_{d,AB}}{R_{d,AB}}\right)}\right]^2 & R_{AB} > R_{d,AB} \end{cases} \tag{1.2}$$

By combining equation 1.1, equation 1.2 and $g(R_{AB})$, a switching function with a value between 0 and 1 (developed for the numerical quadrature in DFT, see reference [6]), the dispersion potential is defined as:

$$V^{SAM}(R_{AB}) = \begin{cases} 0 & R_{AB} \leq R_{d,AB} \\ \frac{C_{6,AB}}{[R_{AB}^2 - R_{d,AB}^2]^3} f(R_{AB}) * g(R_{AB}) & R_{AB} > R_{d,AB} \end{cases} \tag{1.3}$$

Summary
Authors claim to have created a cost-efficient functional which achieves an accuracy comparable to B2PLYP-D3 and CCSD(T), assuming the aug-cc-pVTZ basis set is used. APF-D shows proper long-range interaction, but seems to overestimate binding energies at short distances.

1.1.2 BMK

BMK stands for 'Boese-Martin for Kinetics'. A work by Martin et al. has been taken as literary basis to describe this functional.[7] This functional is specialized for calculations regarding kinetics, for example reaction barriers. These calculation require very accurate exchange correlation energies (E_{XC}). To achieve this, the authors constructed the equations concerning this energy in the following manner:

$$E_{XC} = E_{X,l} + E_{X,n-l} + E_C + aE_{HF} \tag{1.4}$$

- E_X: energy of pure exchange
- E_C: correlation energy
- E_{HF} : Hartree Fock exchange energy
- a: exact exchange mixing coefficient

Note that the energy of pure exchange has been split into a local part (l) and a non-local part (n-l). Equations 1.5 and 1.6 both use a generalized gradient approximation (GGA) as proposed by Becke.[8] This approximation consists of a local spin density

factor $e_{X\sigma}^{LSDA}(\rho_\sigma)$, a reduced spin gradient (s_σ^2) and the gradient enhancement factor $g_{X\sigma}$. Please note that σ represents the α or β spin. In addition to the GGA, equation 1.6 applies a power series expansion $(f_{X\sigma}(w_\sigma))$ to w_σ, a functional for modeling the exchange hole.

$$E_{X,l} = \sum_\sigma \int e_{X\sigma}^{LSDA}(\rho_\sigma) g_{X\sigma,l}(s_\sigma^2) d\mathbf{r} \tag{1.5}$$

$$E_{X,n-l} = \sum_\sigma \int e_{X\sigma}^{LSDA}(\rho_\sigma) g_{X\sigma,n-l}(s_\sigma^2) f_{X\sigma}(w_\sigma) d\mathbf{r} \tag{1.6}$$

The correlation energy is given by the sum of the contributions made by α- and β-spin densities.

$$E_C = E_{C\alpha\alpha} + E_{C\alpha\beta} \tag{1.7}$$

where

$$E_{C\sigma\sigma} = \int e_{C\sigma\sigma}^{LSDA}(\rho_\sigma) g_{C\sigma\sigma}(s_\sigma^2) d\mathbf{r} \tag{1.8}$$

and

$$E_{C\alpha\beta} = \int e_{C\alpha\beta}(\rho_\alpha, \rho_\beta) g_{C\alpha\beta}(s_{avg}^2) d\mathbf{r} \tag{1.9}$$

The major differences between the functionals corresponding to parallel $(\sigma\sigma)$ and the opposite $(\alpha\beta)$ spin are the latter's lack of the local spin density approximation (thus only the density function $e_{C\alpha\beta}$ remains) as well as it's definition of the reduced gradient s_{avg}^2, which is the average of s_α^2 and s_β^2.

Summary
Considering equilibrium properties, BMK performs similar to the best functionals. Compared to B3LYP its geometries and vibrational frequencies are less reliable. The authors view BMK to be a general-purpose functional but with superior performance in regards to calculating transition states. The amount of HF exchange of this functional equals 42%.

1.1.3 CAM-B3LYP

The majority of descriptions about this functional has been taken from the work of T. Yanai and coworkers.[9] CAM-B3LYP is a method which uses the hybrid qualities of B3LYP and combines it with short and long-range corrections. The form of the latter has been suggested by Tawada et al.[10] Both corrections are included by defining the inverse of r_{12}, the distance between two electrons, as follows:

$$\frac{1}{r_{12}} = \frac{1 - [\alpha + \beta * erf(\mu r_{12})]}{r_{12}} + \frac{\alpha + \beta * erf(\mu r_{12})}{r_{12}} \tag{1.10}$$

where μ is a parameter that determines the ratio between HF and DFT exchange and α is a weighting factor for the contribution of the HF exchange. Adding β as an additional parameter allows for the inclusion of a factor for the DFT exchange. This factor is defined as $1 - (\alpha + \beta)$, where $0 \leq \alpha + \beta \leq 1$ and both α and β are positive. The approach has been referred to as the 'Coulomb-attenuating method' or 'CAM'.

The incorporation of the short-range functional is performed by describing the functional of the exchange energy E_x^{sr} according to equation 1.11:

$$E_x^{sr} = \frac{1}{2}\sum_{\sigma}\int \rho_{\sigma}^{4/3} K_{\sigma} \times \left\{1 - \frac{8}{3}a_{\sigma}\left[\sqrt{\pi}erf\left(\frac{1}{2a_{\sigma}}\right) + 2a_{\sigma}(b_{\sigma} - c_{\sigma})\right]\right\} d^3\mathbf{r} \tag{1.11}$$

where

- K_{σ} is the exchange operator
- ρ_{σ} represents the electron density
- $a_{\sigma} = \frac{\mu K_{\sigma}^{1/2}}{6\sqrt{\pi}\rho_{\sigma}^{1/3}}$
- $b_{\sigma} = exp\left(-\frac{1}{4a^{2\sigma}}\right) - 1$
- $c_{\sigma} = 2a^{2\sigma}b_{\sigma} + \frac{1}{2}$

The long range interaction is applied using the HF exchange integral in equation 1.12, in which $\Psi_{i/j\sigma}^*$ represents the i^{th}/j^{th} σ-spin molecular orbital.

$$\begin{aligned} E_x^{lr} = \frac{1}{2}\sum_{\sigma}\sum_{i}^{occ}\sum_{j}^{occ}\int\int \Psi_{i\sigma}^*(\mathbf{r}_1)\Psi_{j\sigma}^*(\mathbf{r}_1) \\ \times \frac{erf(\mu r_{12})}{r_{12}}\Psi_{i\sigma}^*(\mathbf{r}_2)\Psi_{j\sigma}^*(\mathbf{r}_2)d^3\mathbf{r}_1 d^3\mathbf{r}_2 \end{aligned} \tag{1.12}$$

Summary
Three parameters ($\mu = 0.33$, $\alpha = 0.19$ and $\beta = 0.46$) are used to adjust the mixing of DFT and HF exchange. Compared to B3LYP, CAM-B3LYP to exhibits improved long range behaviour at the price of less than twice the computational cost. Additionally, it is useful for charge transfer excitations as well as the calculation of polarizability of long chains.

1.1.4 M06-2X

The majority of information about this functional has been gained from an article by Y. Zhao and D. G. Truhlar.[11] M06-2X is a Minnesota functional of the Minnesota 06 suite, which possesses twice the amount of nonlocal exchange (2X) compared to the M06 functional[11]. The functional possesses three main parameters: the spin density ρ_σ, its reduced gradient x_σ and the spin kinetic energy density τ_σ. The latter two are defined as shown in equation 1.13 and 1.14.

$$x_\sigma = \frac{|\bigtriangledown \rho_\sigma|}{\rho_\sigma^{4/3}} \tag{1.13}$$

$$\tau_\sigma = \frac{1}{2} \sum_i^{occup} |\bigtriangledown \psi_{i\sigma}|^2 \tag{1.14}$$

M06 is a linear combination of M05 and VSXC, the kinetic-energy-dependent exchange-correlation (XC) functional of Voorhis and Scuseria (VS). M06-2X is a special case which does not use the local spin density approximation for exchange described in VSXC, thus reducing the M06 functional to that of M05.[12]

$$E_X^{M05} = \sum_\sigma \int dr \left[F_{X\sigma}^{PBE}(\rho_\sigma, \bigtriangledown \rho_\sigma) f(w_\sigma) \right] \tag{1.15}$$

where

- $F_{X\sigma}^{PBE}(\rho_\sigma)$: exchange energy density of the PBE exchange model
- $f(w_\sigma)$: kinetic-energy-density enhancement factor
- w_σ: a variable which contains functions correlating to τ_σ and ρ_σ

To describe the total correlation energy E_C a M05 and VSXC-based meta-generalized gradient approximation correlation functional is employed.

$$E_X^{M05} = E_{C\alpha\alpha} + E_{C\alpha\beta} + E_{C\beta\beta} \tag{1.16}$$

Functionals describing opposite spins ($\alpha\beta$) possess a different definition than those of parallel-spin ($\alpha\alpha$ or $\beta\beta$): opposite-spin functions contain the reduced spin density gradient x_σ of both α and β, whereas parallel-spin functions only use the gradient of the spin in question. The latter case also possesses a self-interaction correction factor.

M06-2X possesses a HF exchange of 54%, thus the hybrid exchange-correlation energy is expressed as:

$$E_{XC}^{hyb} = \frac{54}{100} E_X^{HF} + \frac{100-54}{100} E_X^{DFT} + E_C^{DFT} \tag{1.17}$$

Summary
Due to the high percentage of HF exchange M06-2X is a comparatively reliable functional for main group kinetics and thermochemistry (much like BMK) as well as noncovalent interactions.

1.1.5 PBE0

The article of C. Adamo and V. Barone, which introduces this functional, was used as main source for the following information.[13] PBE0 is a density functional model which does not contain adjustable parameters. Its name derives from a GGA functional created by Perdew, Burke and Ernzerhof (PBE) and the implementation of the adiabatic connection method with no empirical parameter, ACM0 (0). By combining the Perdew-Wang correlation functional and the exchange contribution E_X^{PBE} shown in equation 1.18 the PBE functional can define every parameter (local spin density aside) as constant.

$$E_X^{PBE} = \frac{bx^2}{1+ax^2} \tag{1.18}$$

where

$$x = \frac{|\bigtriangledown\rho|}{\rho^{4/3}} \tag{1.19}$$

The variables in the equations are defined as follows:

- a: a factor of 0.00449
- b : a factor of 0.00336
- ρ: electron density
- $\bigtriangledown\rho$: electron density gradient

To mix HF and DFT exchange, the adiabatic connection formula was used and applied to the exchange correlation. Becke suggested that the formula only required a single parameter to represent the ratio between HF and DFT exchange, which gave rise to the adiabatic connection methods with one empirical parameter (ACM1). Perdew et al. showed that by predetermining this parameter (ACM0) accurate results are still achievable - granted that fourth-order pertubation theory is used. In the case of PBE0, this parameter is set to $1/4$ as depicted in equation 1.20. In other words, this method possesses a HF exchange of 25%.

$$E_{XC}^{ACM0} = E_{XC}^{GGA} + \frac{1}{4}(E_X^{HF} - E_X^{GGA}) \tag{1.20}$$

Summary
PBE0 has been described to generally perform comparable to mPW0. It can be used for all elements and bigger systems. This is due to the lack of adjustable parameters which considerably cut computation costs. The functional also possesses good accuracy regarding the prediction of excitation energies.

1.2 Basis Sets

This section contains information about the basis sets employed in this thesis. Generally speaking, a basis set consists of functions - referred to as basis functions - which describe a vector space. This space sets the boundaries in which a mathematical problem is solved. In quantum chemistry, the vector space is the wave function of a molecular orbital, which is constructed by a linear combination of basis functions.

1.2.1 Pople Basis Sets

Information about the Pople basis set was taken from reference [1]. The Pople basis set is named after its creator, J. A. Pople, a famous theoretical chemist. Pople's split valence basis sets possess a nomenclature in the form of x-yG. 'x' represents the number of Gaussian functions (G) used for each orbital basis function of a core atom, 'y' contains a number for each basis function in the split valence basis set. For example: the double-zeta basis set is 6-31G, which means that six Gaussians are used for one basis function and each split valence orbital is composed of two basis functions (31) which are linear combinations of 3 and 1 Gaussian functions, respectively. These basis sets can be augmented with diffusion and polarization functions:

Polarization function:
With regards to their geometry, molecular orbitals require more flexibility than atom orbitals. This is achieved through the addition of a function describing an orbital with $l + 1$, where l is the angular quantum number of the atom's valence orbital. Therefore, s-orbitals ($l = 0$) are polarized by a p-orbital function ($l = 1$), p-orbitals by d-orbital functions ($l = 2$), et cetera. The letter corresponding to the orbital described by the polarization function is then added in parenthesis after the rest of the Pople basis set. For hydrogen and 6-31G as basis set, the valence orbital is an s-orbital ($l = 0$), thus it is polarized by a p-orbital ($l = 1$). The required basis set is then 6-31G(p). For larger atoms (C,N,...) this is analog to 6-31G(d).

Diffuse function:
Due to weakly bound electrons, some molecular orbitals (MO) require additional functions to describe a greater spatial distribution of electron density to avoid significant energetical errors. Such functions are called diffuse functions and they are usually designed with smaller exponents than the valence functions of the basis set. One can add up to two diffusion functions to a basis set, which is denoted by a '+' between y and G for each. For instance, two diffusion functions added to the 6-31G(p) basis set would be written as 6-31++G(p). The first diffusion function adds one s function and a set of p functions to all atoms except H and He, whereas the second provides an additional s function to hydrogens.

1.2.2 Correlation-consistent Basis Sets

The correlation-consistent basis set was created by Dunning et al., whose work has been used as source for this subsection.[14] For both HF and electron correlation calculations, these basis sets optimize exponents and contraction coefficients - it is thus 'correlation-consistent'(cc). Its different sets are denoted cc-pVnZ, whereas n represents the letter/number (see Table 1.1) corresponding to the number of basis functions (zetas, Z) used for each valence orbital (V). Please note that all of the presented rules are restricted to atoms H to Ar.

Table 1.1: Signs corresponding to the number of basis functions used for each valence orbital

Number of basis functions	2	3	4	5	6
Sign replacing "n"	D	T	Q	5	6

These basis sets include polarization functions and contracted functions. The set of contracted functions consists of the atoms's regular orbitals and additional orbital functions. For each basis function beyond the first ($n-1$), one orbital function of an orbital type (s/p/d/f), which is already present in the regular atom orbitals, will be added.

For instance, cc-pVTZ is a triple-zeta correlation-consistent basis set and thus possesses three basis functions per orbital function (n = 3). Therefore, the contracted functions of carbon include the regular 1s2s2p orbital functions and addtionally two s- and two p-orbital functions, as the regularly present orbital types are s and p and the number of each added orbital type is $n-1$.

Polarization function:
Rather than adding a single orbital function of a higher angular quantum number, this approach adds a set of polarization functions (P_{set}) according to equation 1.21:

$$P_{set} = \sum_{x=1}^{n-1} x * F_{l+n-x} \tag{1.21}$$

whereas

- n is the number of zetas
- l is the highest angular quantum number within the period

- *F* is the function corresponding to an orbital with the angular quantum number l+n-x

To depict this behavior, Table 1.2 has been created.

Table 1.2: Contracted and polarization functions corresponding to basis set and period.

	H - He		Li - Ne		Na - Ar	
Zeta	Contr.	Pol.	Contr.	Pol.	Contr.	Pol.
cc-pVDZ	[2s]	[1p]	[3s 2p]	[1d]	[4s 3p]	[1d]
cc-pVTZ	[3s]	[2p 1d]	[4s 3p]	[2d 1f]	[5s 4p]	[2d 1f]
cc-pVQZ	[4s]	[3p 2d 1f]	[5s 4p]	[3d 2f 1g]	[6s 5p]	[3d 2f 1g]

Diffusion function:
The basis set can be augmented with diffuse functions; the prefix 'aug-' is then added to the name of the basis set. Their concept is similar to those of the Pople diffuse functions, but one diffuse function is added to each angular momentum (s,p,d,..) present according to Table 1.2.

1.2.3 Karlsruhe Basis Sets

The information about this basis set was taken from 'Balanced basis sets of split valence, triple zeta valence and quadruple zeta valence quality for H to Rn: Design and assessment of accuracy', by Weigend and Ahlrichs.[15] The Karlsruhe basis sets possesses two designs and thus two nomenclature patterns:

- def2-SV:
  The 'def2' stems from the 'def' in the TURBOMOLE basis set library of this basis sets predecessor. To denote this as the successor, a 2 was added.
  'SV' stands for 'split valence', denoting that core atom orbitals use only one basis function and valence atom orbitals employ a larger basis.
- def2-nZV:
  The prefix exists for the same reason as stated above. Unlike the SV approach, several basis functions are used for valence atom orbitals. The suffix 'nVZ' represents this approach, as 'VZ' stands for 'zeta valence' and 'n' denotes the number of basis functions used - D for double, T for triple and Q for quadruple.

Polarization function:
The addition of polarization functions is denoted by the 'P' at the end of the basis set, but is is also possible to use a greater set of polarization functions by attaching another 'P'.

Diffusion function:
After defining the polarization functions, one can choose to add diffusion functions by adding a 'D' at the end of the basis set name.

1.3 Employed Basis Sets

The basis sets used in this work are shown in Table 1.3. The correlation-consistent basis set possesses the greatest number of functions, whereas the Pople basis set possesses the least. It is noteable that the latter does not augment the hydrogen atoms with a p-orbital function.

Table 1.3: Comparison of used basis sets. Numbers represent the total number of orbital functions, not the cordial numbers.

Basis set	**aug-cc-pVTZ**	**def2-TZVP**	**6-311+G(d)**
H	4s 3p 2d	3s1p	3s
C/N/O/F	5s 4p 3d 2f	5s 3p 2d 1 f	5s 4p 1d

1.4 Continuum Solvation Models

This section introduces the concept of continuum solvation and the models employed in this work. Cramer's 'Essentials of Computational Chemistry: Theories and Models' [1] was used as source material for the information given below. Using explicit solvent molecules can be a very costly enterprise, especially for larger molecules and/or basis sets. Even if used, there is no guarantee that the solvation shells are accurately modeled nor that the 'edge effects' of the outer solvent molecules are negligible. Another ansatz is to place the solute molecule

into a (dielectric) continuous medium and create a cavity.
This approach is named 'implicit solvation' or 'continuum solvation' and only applies for condensed phase systems.

When introducing the solute in a solvent the solutes charge distribution of the solvent and the solute interact with each other. This introduction of the solute into the continuum starts a cycle of 2 steps:

1. the polarity of the solute increases due to the field of the solvent
2. the solvent is polarized by the solute and arranges its orientation opposite to the solute's dipole

The cycle ends once the energy requirement for the increase of the polarization is equal to the energy gained from the additional polarization. In the case of a continuum solvation model, a continuous electric field is used instead of the solvents charge distribution. This electric field is defined using a gradient of the electrostatic potential ϕ and is referred to as 'reaction field'. The energy required to increase the polarity (which is the same as distributing charges), G, is defined as

$$G = -\frac{1}{2}\int \rho(\boldsymbol{r})\phi(\boldsymbol{r})d\boldsymbol{r} \tag{1.22}$$

where ρ is the solute's charge density and $\boldsymbol{r}$ the location in the field.

The free polarization energy, G_P, is the difference between the energy required for the polarization in gas phase and solution. Assuming the solute is a monoatomic ion with a dipolar distribution, this can also be expressed with the Kirk-Onsager equation:

$$G_P = -\frac{1}{2}\left[\frac{2(\varepsilon-1)}{2\varepsilon+1}\right]\frac{\mu^2}{a^3} \tag{1.23}$$

where the gas phase possesses a dielectric constant of 1 and for the solvent the dielectric constant is ε. μ is the dipole moment and a is the radius of the ion's spherical cavity.

The Schrödinger equation in solution for the case formulated in equation 1.23 can be expressed as:

$$\left\{H - \frac{1}{2}\left[\frac{2(\varepsilon-1)}{2\varepsilon+1}\right]\frac{\langle\Psi|\mu|\Psi\rangle}{a^3}\mu\right\}\Psi = E\Psi \tag{1.24}$$

where μ in equation 1.24 represents the dipole moment operator, H is the gas phase Hamiltonian and Ψ is the wavefunction of the molecule orbitals. Solving the Kohn-Sham equations (in the case of DFT calculations) while accounting for the solvation can result in a non-linear Schrödinger equation, like formula 1.24. Such a formulation can be solved by a self-consistent reaction field (SCRF) calculation. In the SCRF formalism, the lowering of energy due to an increased dipole moment leads to an increased energy of the gas phase Hamiltonian. The state of a stationary solution is achieved once these two energies would be the same upon increasing the dipole.

1.4.1 Polarizable Continuum Model

Most of the information given in this subsection was taken from "Electrostatic interaction of a solute with a continuum. A direct utilization of ab initio potentials for the prevision of solvent effects.", by Miertus, Scrocco and Tomasi. [16] The calculation process of the polarizable continuum model (PCM) is divided in four major steps:

1) To mimic solute-solvent interaction, this solvent model defines a so-called cavity around the solute. This cavity's surface S consists of spheres K_i, which are further separated into the smaller sections ΔS_{K_i} which are located at s. Each surface element contains a point charge q. For the start of the computation (0^{th} iteration, which is the determination of a set of values) the charge density of a surface element K_i at the position s is

$$\sigma^{00}_{s_{K_i}} = -\left[\frac{\epsilon - 1}{4\pi\epsilon}\right](E^0_p(s_{K_i})_n \tag{1.25}$$

where i is the index for the surface element, ϵ is the dielectric constant of the medium and E^0_p is the electric field generated by the solute charge distribution $p^0(r)$. The first 0 indicates that the unperturbed solute charge distribution, $p^0(r)$, is kept constant.The second stands for the start of the calculation (0^{th} iteration), at which the additional contribution of the electric field generated by the surface charges is not yet used.

2) In each iteration m of this step point charges are evaluated according to the formula:

$$q^{0,m}_{K_i} = \sigma^{0,m}_{s_{K_i}} \Delta S_{K_i} \tag{1.26}$$

An additional contribution to the electric field, $E_\sigma^{0,m}$, is generated by these charges at the center n of each surface element. By incorporating this, each iteration improves σ, which is now defined as:

$$\sigma_{s_{K_i}}^{0,m+1} = -\left[\frac{\epsilon - 1}{4\pi\epsilon}\right](E_p^0 + E_\sigma^{0,m})_n \tag{1.27}$$

(3) The set of point charges of step 2 change the solute charge distribution $p^m(r)$ to increase the polarization, resulting in the new charge distribution $p^{m+1}(r)$. The latter is achieved by solving the following Hamiltonian:

$$H = H^0 + V_\sigma \tag{1.28}$$

where H^0 is the solute Hamiltonian and V_σ is the electrostatic potential produced and perturbed by the surface charges $q_{K_i}^{0,m}$.

(4) Step 2 and 3 are repeated until the system is self-consistent.

1.4.2 Conductor-like Polarizable Continuum Model

Two articles by Barone et al. were chosen as main sources for the description of this continuum solvation model.[17][18] The conductor-like polarizable continuum model (CPCM) is a PCM-based solvation model. In CPCM, cavities are treated differently and formal charge, hybridization and some other effects are taken into account. Most of these considerations are introduced via a CPCM term which corrects the Fock matrix and polarizes the continuum solvent. This and some other implementations result in several differences to the PCM-model:

- the molecular energy is calculated in a more accurate and efficient way
- CPCM implicitely accounts for the charge density outside of the cavity and thus does not require a correction after the calculation
- the linear scaling of the cavity formation allows CPCM to be applied to very big systems

To create the cavity, the universal force field (UFF) is employed.[19] This model possesses a set of fundamental parameters which depends only on the element, the connectivity and the hybridization. The original version of CPCM used the united atom model for Hartree–Fock (UAHF), which is unfit for pK_a calculations as the model does not provide hydrogen atoms with their own spheres.

1.4.3 Solvation Model based on Density

The information presented has been taken from a work by Marenich and his coworkers.[20] SMD is a universal solvent model based on the interaction of a continuum solvent with a solute molecule's quantum mechanical charge density. It is important to note that unlike PCM and C-PCM, no partial atomic charges are defined.

This solvent model defines the free energy of solvation (ΔG°_{solv}, in standard state) as show in equation 1.29:

$$\Delta G^{\circ}_{solv} = \Delta G_{ENP} + G_{CDS} \tag{1.29}$$

ΔG_{ENP} is the free energy corresponding to electrostatic (E), nuclear (N) and polarization (P) contributions. Changes concerning the solvents cavity (C), the dispersion energy (D) as well as the structure (S) of the local solvent are summarized in G_{CDS}.

If the solute geometries in gas phase and liquid phase are the same, then the nuclear contributions can be neglected and ΔG_{ENP} becomes ΔG_{EP}. By assuming the solvent molecule to be rigid, the latter term can be described as:

$$\Delta G_{EP} = \left\langle \Psi | H^{(0)} - \frac{e}{2}\varphi | \Psi \right\rangle + \frac{e}{2}\sum_{k} Z_k \varphi_k - \left\langle \Psi^{(0)} | H^{(0)} | \Psi^{(0)} \right\rangle \tag{1.30}$$

where

- k denotes a specific atom
- e is the elementary charge
- φ is the reaction field
- Z_k equals the atomic number of atom k
- Ψ is the polarized solute electronic wave function
- $\Psi^{(0)}$ represents the gas phase electronic wave function
- $H^{(0)}$ is the solute eletronic Hamiltonian in gas phase

ΔG_{CSD} is defined as shown in formula 1.30. The surface tension and the solvent-accessible surface area (SASA) of atom k are denoted σ_k and A_k, respectively. A_k is determined via R_{Z_k}, the set of atomic van der Waals radii, the geometry R plus the solvent radius r_s, which is equal to 0.4 Å.

$$\Delta G_{CSD} = \sum_k \sigma_k A_k(R, \{R_{Z_k} + r_s\}) + \sigma^M \sum_k A_k(R, \{R_{Z_k} + r_s\} \tag{1.31}$$

It is notable that this solvent model treats water as a special case; it possesses its own surface tension coefficients as well as a molecular surface tension σ^M of zero. SMD is slightly less accurate than its predecessor, SM8, but as an advantage it does not depend on the accurate description of charges. Notably, it already includes CSD terms (caviation, dispersion and repulsion).

1.5 Computational Details

Computations were conducted using the Gaussian09 package.[21]
The geometry optimization as well as the frequency calculations on 2-naphthol (2N), 4-nitrophenol (4NP) and ciprofloxacin (CIP) were conducted using APFD, BMK, CAM-B3LYP, M06-2X and PBE0.[5][7][9][11][13] These calculations were paired either with the basis set aug-cc-pVTZ or with a Pople basis set.[14][22] Harmonic frequency calculations were performed to check the minimum quality of the geometry (no imaginary frequencies are present). For 2N and 4NP, computations included the neutral and anionic form, whereas for CIP several neutral conformations and the protonation states from anionic to tricationic forms have been calculated - both in gas phase and in water.

Condensed phase calculations employed a continuum solvent model, of which three were tested: IEF-PCM, CPCM and SMD.[23][17][20] Results from these calculations were used to predict ground state pK_a values by applying the Born-Haber cycle and via direct calculation.[24][25][26][27] These calculations were carried out using three reaction schemes:

$$HA \rightleftharpoons A^- + H^+ \tag{1.32}$$

$$HA + HO^- \rightleftharpoons A^- + H_2O \tag{1.33}$$

$$HA + H_2O \rightleftharpoons A^- + H_3O^+ \tag{1.34}$$

Electronic transitions were calculated by TD-DFT method using the aforementioned DFT functionals and the basis sets def2-TZVP and 6-311+G(d).[15] All of these calculations were carried out using SMD to mimick the influence of the solvent (water) on the transitions.

The transitions were used to model UV-Vis spectra and to calculate the excited state acid dissociation constant, pK_a^*. This was achieved by using the ground

state pK_a calculated with reaction 1.32 and adding the difference between the ground and excited state acidity, Δ pK_a. The latter is computed by applying the absorptions/emissions calculated according to the linear response (LR), the corrected linear response (cLR) and the state-specific (SS) formalism to the Förster cycle.[28][29][30][31] To simulate the absorption spectra, a Gaussian broadening HWHH parameter was applied with the programm orca_asa or gabedit.[32][33] .

2 Nomenclature

In case of ciprofloxacin (CIP) several conformations are possible. The following nomenclature is used throughout this work as shown below (Figure 2.1). The nomenclature assumes the molecule to be aligned as shown in picture 2.1 and that the quinoline is inside the plane of the paper. The term 'upwards' refers to a position between the plane and the reader, 'downwards' describes a position behind the paper.

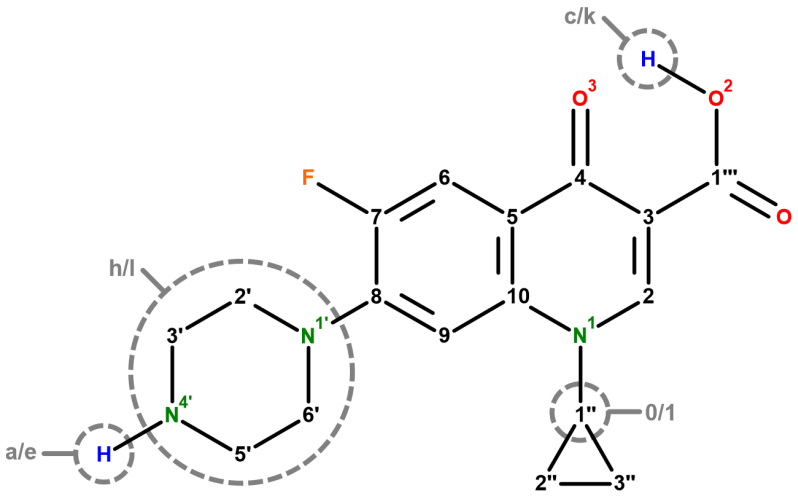

Figure 2.1: Nomenclature of ciprofloxacin in this work

The nomenclature of each form of ciprofloxacin consists of two parts: the protonation state and the conformation. The protonation state is defined as follows:

- CIP^- : anionic form with a single negative charge
- CIPH (n) : neutral form without charge separation
- CIPH (z) : neutral zwitterion
- $CIPH_2^+$: cationic form with a single positive charge
- $CIPH_3^{2+}('4)$: dication with the 2^{nd} protonation at '4
- $CIPH_3^{2+}(1)$: dication with the 2^{nd} protonation at 1
- $CIPH_4^{3+}$: tricationic form

The conformational nomenclature consists of 4 abbreviations:

- **0/1:** Describes the position of the cyclopropane ring relative to the aromatic plane. If the hydrogen on carbon ″1 points upwards then the sign is '0', else it is '1'.

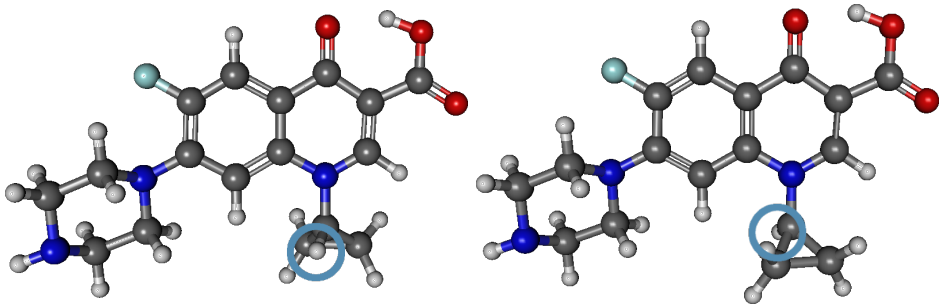

- **h/l:** describes the position of the pyrazine, seen from the same perspective as figure 2.1. If the angle 8-2′-H(2′) is 70-100 degrees, the sign is 'h' (left), else it is 'l' (right). H(2′) denotes the axial hydrogen at the 2′ carbon.

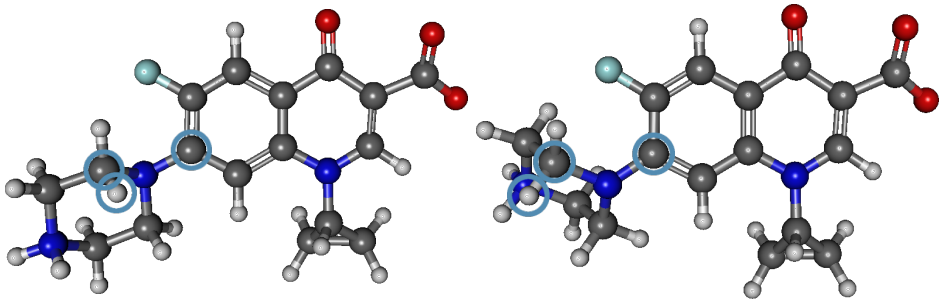

- **a/e:** describes the position of the hydrogen at N′4 for anions and neutral molecules. If the hydrogen is in axial position, the sign is 'a', otherwise it is 'e' for equatorial.

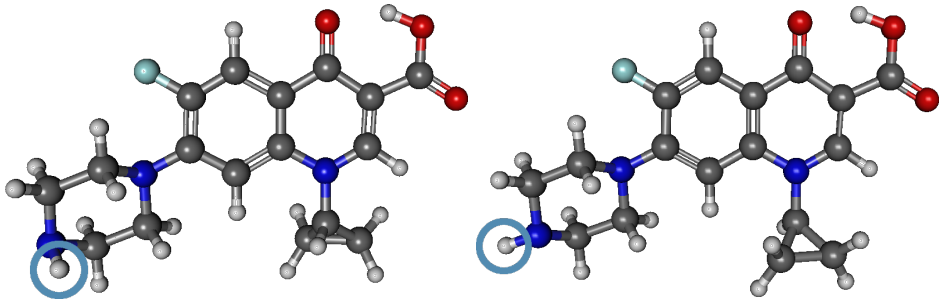

- **c/k:** If the hydrogen atom of the carboxylic group points towards the group's double-bonded oxygen it is 'c', if it points to the ketone it is'k'.

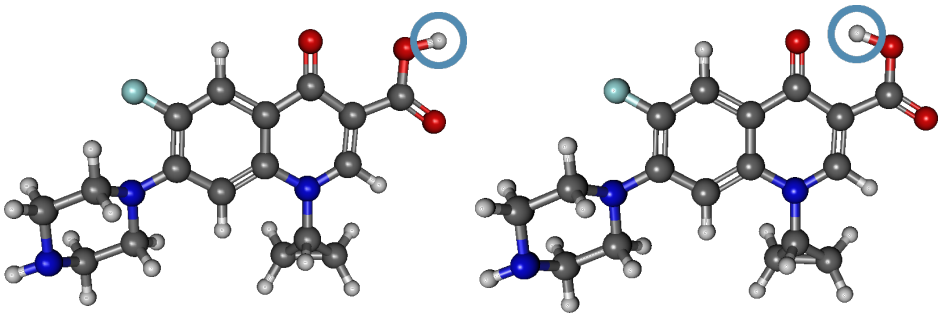

3 Workflow

(1) Several conformations of the neutral and zwitterionic forms of ciprofloxacin have been refined using M06-2X/6-31+G(d). The optimization was conducted in gas phase and condensed phase (water), where the latter employed SMD as the solvation model. The resulting structures were used to conduct frequency calculations with the same method and basis set. By comparing the Gibbs free energies of the conformers, the two thermodynamically favoured ones, N6 and Z3 (see Figure 3.2), have been chosen for further calculations.

(2) After calculating the UV-Vis spectra as well as the acid dissociation constants of the compounds, it was clear that M06-2X/6-31+G(d) lacked the required accuracy for both tasks. Thus, we chose to find the best combination of solvent model, DFT method and (Pople) basis set. In the following five steps.

(3) The solvent models SMD, IEF-PCM and CPCM have been compared using pK_a calculations for 2-naphthol. The one closest to the experimental pK_a has been chosen for all further calculations in solvation.

Figure 3.1: Depiction of the workflow

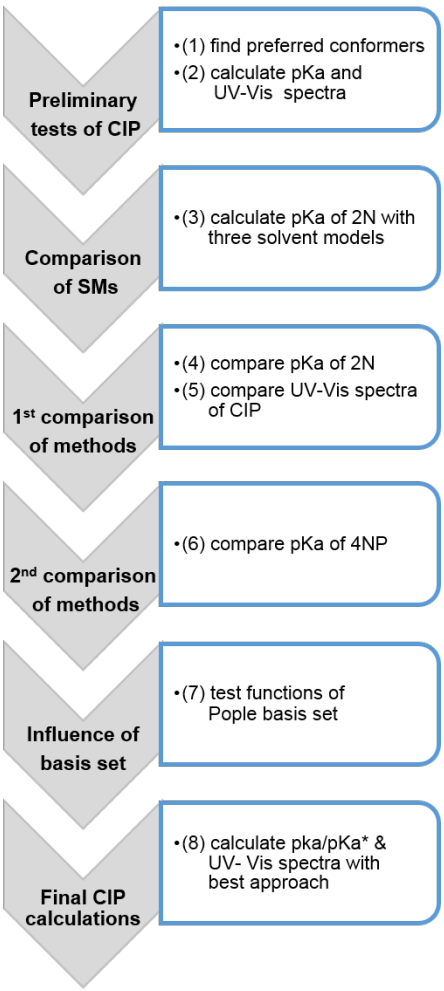

Next, the DFT methods APFD, BMK, CAM-B3LYP, M06-2X and PBE0 have been tested and compared. The first set of tests includes two main parts:

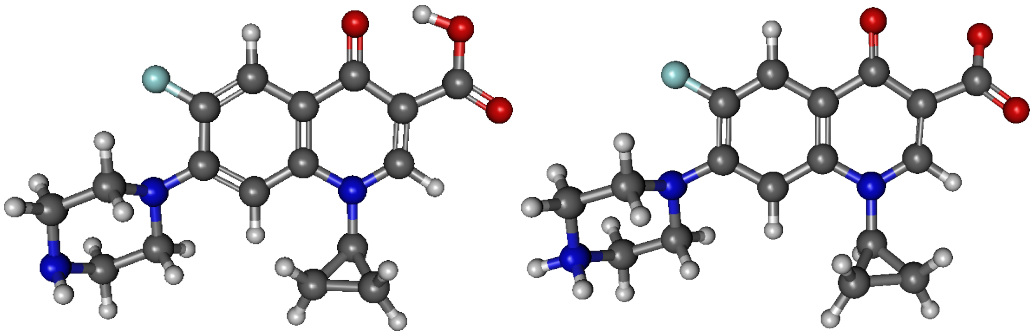

Figure 3.2: Preferred neutral (left) and zwitterionic forms (right) of CIP

(4) One test is the computation of 2-naphthol's acid dissociation constant in the ground (pK_a) and excited state (pK_a^*). For this purpose, 6-311+G(d) was used as basis set and SMD as solvation model.
The Förster cycle was employed to obtain the change of acidity, ΔpK_a. The latter was computed using the corresponding absorption/emission band of the acid and its conjugated base. pK_a^* is then calculated by adding this difference to the ground state acid dissociation constant. The pK_a^* was obtained via three ways, whereby used one of the following formalisms to obtain absorption and emission bands: linear response (LR), corrected linear response (cLR) and state specific (SS).

(5) The other test is the comparison of UV-Vis spectra of CIP obtained by the five DFT functionals with experimental spectra. These calculations applied geometries obtained by M06-2X/6-31+G(d) without further optimization. def2-TZVP was used as basis set.

(6) Employing the three DFT methods which overall performed best in steps 4 and 5, ground state pK_a calculations were conducted for 4-nitrophenol. Basis set and solvent model were the same as in step 4.

(7) Three aspects of the Pople basis set have been tested with regard to their influence on the pK_a using the basis set which performed best through steps 4 to 6:
1. the change from double-ζ to triple-ζ (6-31 to 6-311)
2. the change from one diffuse function to two (+ to ++)
3. the change from (d) to (d,p)-polarization function

From all these tests, CAM-B3LYP/6-311+G(d)/SMD has been determined as the overall best approach for all planned tasks.

(8) Several aspects of the protonation states of ciprofloxacin (anionic to tricationic) have been calculated using the previously mentioned approach, including acid dissociation constants, the protonation pathway and UV-Vis spectra. Geometry optimization and frequency computation of all compounds, pK_a calculations and the prediction of their absorption bands was performed for CIP.

4 Conformations of Ciprofloxacin

Table 4.1 depicts the differences in energy between several stereoisomers of ciprofloxacin. Looking at the Gibbs free energy at 298 K several trends can be observed:

- in gas phase, zwitterions are highly unfavoured, but in SMD their energy is comparable to the neutral forms
- regarding the cyclopropane moiety, '1' is favoured over '0' in SMD
- on average, the 'H' conformere of the piperazin group is energetically preferredin SMD
- on average, solvent phase conformers with an axial hydrogen at N'4 ('a') possess lower energy than the equatorial conformers

Please note that the most stable isomer in solution, N(6)1Huk, has been added later in the study and is therefore not included in earlier calculations regarding ciprofloxacin.

Table 4.1: Comparison of energies of ciprofloxacin-conformers. Energies in kJ/mol were obtained using M06-2X/6-31+G(d). N denotes neutral and Z denotes zwitterionic forms.

Relative Energies [kJ/mol]					Gas Phase			Solvation: SMD		
Conformere					G298	E_{el}	E_{el}+ZPE	G298	E_{el}	E_{el}+ZPE
N_1	o	l	a	c	31.94	35.48	34.58	16.51	21.22	22.11
N_2	o	l	a	k	3.88	3.89	3.66	17.70	15.55	16.70
N_3	o	h	a	k	3.89	3.89	3.66	5.05	-0.74	2.15
N_4	o	h	e	c	28.88	31.95	31.36	26.29	21.80	24.85
N_5	o	h	e	k	0.00	0.00	0.00	6.42	0.44	3.10
N_6	1	h	a	k	3.94	4.68	4.33	0.00	0.00	0.00
N_7	1	h	e	k	0.94	0.28	0.76	3.20	1.35	2.60
Z_1	o	h	n	n	367.74	373.87	372.35	26.19	16.87	24.56
Z_2	o	h	n	n	367.25	373.55	372.13	12.17	1.65	10.44
Z_3	1	h	n	n	367.41	374.25	372.59	6.99	3.25	8.60

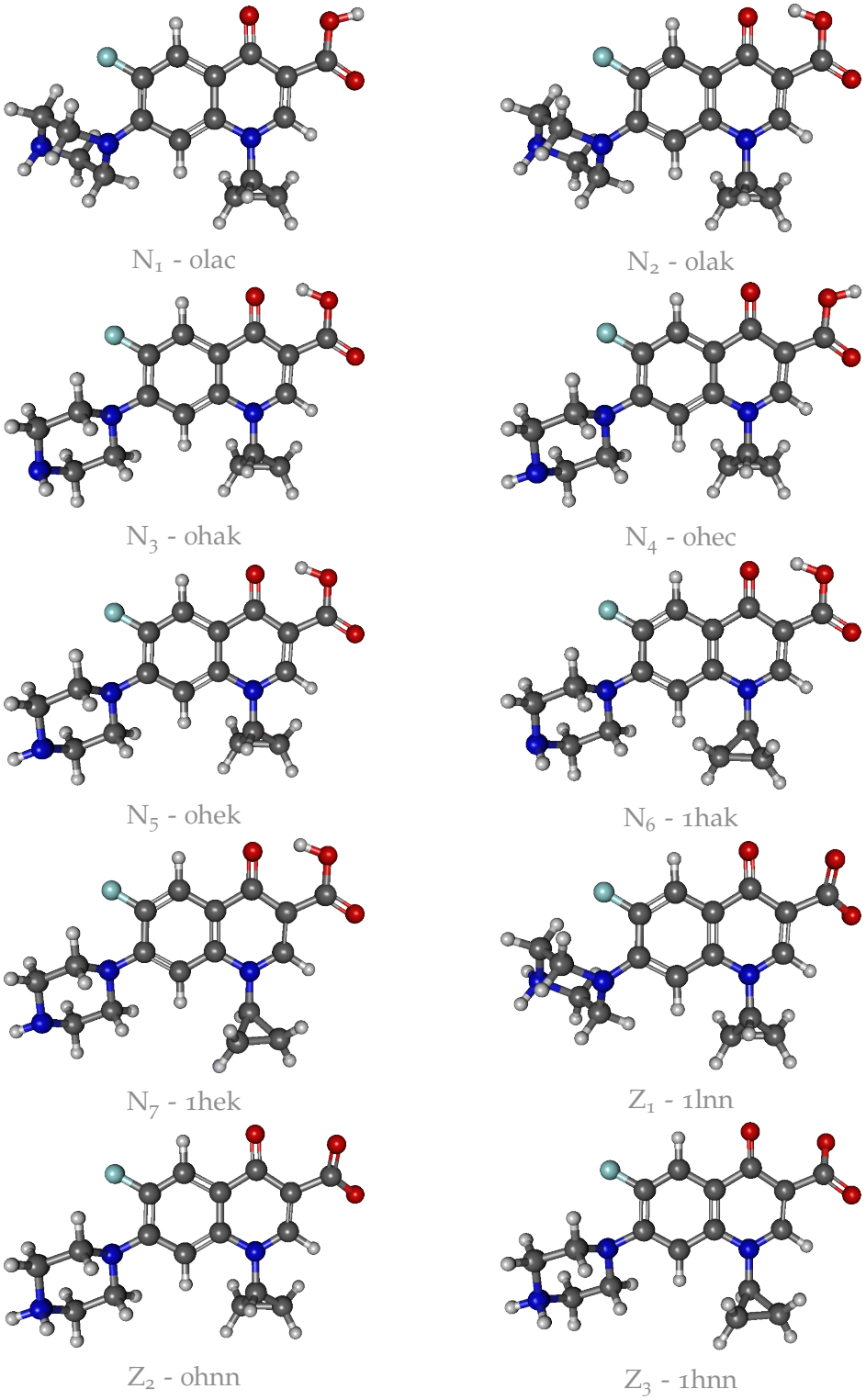

Figure 4.1: Tested conformers of ciprofloxacin with total neutral charge

The relative energies shown in Table 4.2 clearly show that zwitterionic structures ($CipH_{(N4')}$ and $CipH_2{}^{+}{}_{(N4', N1)}$) are clearly unfavoured in the gas phase. When comparing the relative energies of the dications in gas phase and condensed phase (Table 4.3), it is evident that different conformers are preferred - $CipH_3{}^{2+}{}_{(N4', N1', OH)}$ in solution and $CipH_3{}^{2+}{}_{(N4', N1, OH)}$ in the gas phase. Additionally the energetical difference between the favoured and the unfavoured dicationic conformers is significantly smaller in the gas phase.

Table 4.2: Gas phase energies of CIP. Energies relative to tautomers of the same protonation state are given in kJ/mol.The used approach was CAM-B3LYP/6-311+G(d).

	Absolute Energies [Eh]			Relative Energies [kJ/mol]		
Conformeres	**Δ G_{gas}**	**E_{gas}**	**ZPE_{gas}**	**Δ G_{gas}**	**E_{gas}**	**ZPE_{gas}**
$CipH_4{}^{3+}{}_{(N4', N1', N1, OH)}$	-1148.50291	-1148.83363	0.38201	- - -		
$CipH_3{}^{2+}{}_{(N4', N1', OH)}$	-1148.41076	-1148.73062	0.37022	4.04	2.06	7.89
$CipH_3{}^{2+}{}_{(N4', N1, OH)}$	-1148.41230	-1148.73140	0.36936	0.00	0.00	5.63
$CipH_3{}^{2+}{}_{(N1', N1', OH)}$	-1148.37887	-1148.69486	0.36721	87.76	95.95	0.00
$CipH_2{}^{+}{}_{(N4', OH)}$	-1148.21276	-1148.52022	0.35669	0.00	0.00	3.95
$CipH_2{}^{+}{}_{(N4', N1)}$	-1148.02234	-1148.32590	0.35519	499.95	510.19	0.00
$CipH_{(N4')}$	-1147.73471	-1148.02569	0.34164	353.58	358.86	0.00
$CipH_{(OH)}$	-1147.86938	-1148.16237	0.34178	0.00	0.00	0.36
Cip^-	-1147.32252	-1147.59937	0.32709	- - -		

Table 4.3: Energies of CIP in aqueous solution. Energies relative to tautomers of the same protonation state are given in kJ/mol.The used approach was CAM-B3LYP/6-311+G(d)/SMD.

	Absolute Energies [Eh]			Relative Energies [kJ/mol]		
Conformers	**Δ G_{smd}**	**E_{smd}**	**ZPE_{smd}**	**Δ G_{smd}**	**E_{smd}**	**ZPE_{smd}**
$CipH_4{}^{3+}{}_{(N4', N1', N1, OH)}$	-1149.12598	-1149.46186	0.38565	- - -		
$CipH_3{}^{2+}{}_{(N4', N1', OH)}$	-1148.77113	-1149.09554	0.37234	0.00	0.00	4.63
$CipH_3{}^{2+}{}_{(N4', N1, OH)}$	-1148.71583	-1149.03706	0.37072	145.20	153.55	0.39
$CipH_3{}^{2+}{}_{(N1', N1', OH)}$	-1148.69145	-1149.01325	0.37058	209.21	216.07	0.00
$CipH_2{}^{+}{}_{(N4', OH)}$	-1148.35744	-1148.66488	0.35668	0.00	0.00	0.00
$CipH_2{}^{+}{}_{(N4', N1)}$	-1148.33049	-1148.63978	0.35882	70.77	65.91	5.63
$CipH_{(N4')}$	-1147.91145	-1148.20612	0.34382	0.45	0.00	6.81
$CipH_{(OH)}$	-1147.91162	-1148.20345	0.34123	0.00	7.00	0.00
Cip^-	-1147.46493	-1147.74437	0.32859	- - -		

All mono-, di- and tri-cations were calculated using the conformation 'hak' . Their relative energies depending on the '0/1' conformation are displayed in Table 4.4. No general preference of the '0' or '1' conformation for gas or condensed phase was observed.

Table 4.4: Comparison of phases and and the 0/1 conformation among cations of CIP using CAM-B3LYP/6-311+G(d)/SMD.

G^{298} [Eh]				
Solvation	Conformation	Cation	Dication	Trication
Gas	1	-1148.212759	-1148.410763	-1148.502906
	0	-1148.212913	-1148.410218	-1148.502359
SMD	1	-1148.357443	-1148.77113	-1149.125977
	0	-1148.356876	-1148.772148	-1149.123216
ΔG^{298} [kJ/mol]				
Phase	Conformation	Cation	Dication	Trication
Gas	1	0.40	0.00	0.00
	0	0.00	1.43	1.44
SMD	1	0.00	2.67	0.00
	0	1.49	0.00	7.25

5 Calculation of the pK$_a$

This chapter presents the mathematical background regarding the calculation of the acid dissociation constants.

5.1 General

A major part of this work is the pK$_a$ calculation of the fluoroquinolone CIP. Each compound described in this work can act as Brønsted–Lowry acid, meaning it is able to donate a proton to its reaction partner/solvent – a reaction, in which the educt (HA) results in its conjugated base (A^-). The general reaction scheme for the hydrogen abstraction from an acid is described as follows:

$$HA \rightarrow H^+ + A^- \tag{5.1}$$

The greater the preference for the products in equilibrium, the higher the compound's acidity. The extend of this acidity is quantified via the acid dissociation constant K_a:

$$K_a = \frac{[A^-][H^+]}{[HA]} \tag{5.2}$$

The negative decadic logarithm of this constant is called the pK$_a$:

$$pK_a = -log(K_a) \tag{5.3}$$

As with all reactions, the equilibrium between the two sides of a reaction is governed by the difference of their Gibbs free energy and the temperature. In our case, this energy will be referred to as ΔG_{aq}, as our reaction is assumed to occur in water.

$$\frac{\Delta G_{aq}}{RT} = -ln(K_a) \tag{5.4}$$

By applying the negative decadic logarithm to equation 5.4 we obtain the mathematical definition for the pK_a :

$$pK_a = \frac{\Delta G_{aq}}{RTln(10)} \tag{5.5}$$

It follows from equation 5.5, that at standard ambient temperature and pressure a difference of 5.7 kJ/mol equals one pK_a unit. Therefore, the calculation of ΔG_{aq} has to be quite accurate. In the case of the reaction in equation 5.1, the resulting definition of ΔG_{aq} is:

$$\Delta G_{aq} = G_{aq}(A^-) + G_{aq}(H^+) - G_{aq}(HA) \tag{5.6}$$

While this equation appears to be rather simple, obtaining accurate values for G_{aq} remains a difficult task, which is mainly due to the lack of an accurate description of molecules in solvation. Due to limitations of time and resources available to research, it is important to find approaches for pK_a calculations which provide the necessary accuracy without the use of big basis sets or extensive methods – especially when computing larger molecules.

5.2 Thermodynamic Cycles

As previously mentioned, the reliable and accurate computation of energies for molecules in the solvent phase proves to be difficult to achieve, but it can be avoided through the use of a thermodynamic cycle. In general, a thermodynamic cycle describes a number of sequential thermodynamic processes, which ultimately return the system to its original state. For calculations including solvated protons, literature values are taken.

5.2.1 The Born-Haber Cycle

The Born-Haber cycle is a thermodynamic cycle which is commonly used for pK_a calculations. [24][25]. It uses Hess's law of constant heat summation, which states that the change of the total enthalpy of a chemical reaction is always the same, regardless of how the final state was achieved. This law is applied by splitting the energy of any compound in solution into the gas phase energy G_{gas} and the Gibbs free energy of solvation ΔG_S. This can be expressed as:

$$G_{aq} = G_{gas} + \Delta G_s \tag{5.7}$$

If this is done for every individual compound of equation 5.1, the thermodynamic cycle can be depicted as follows:

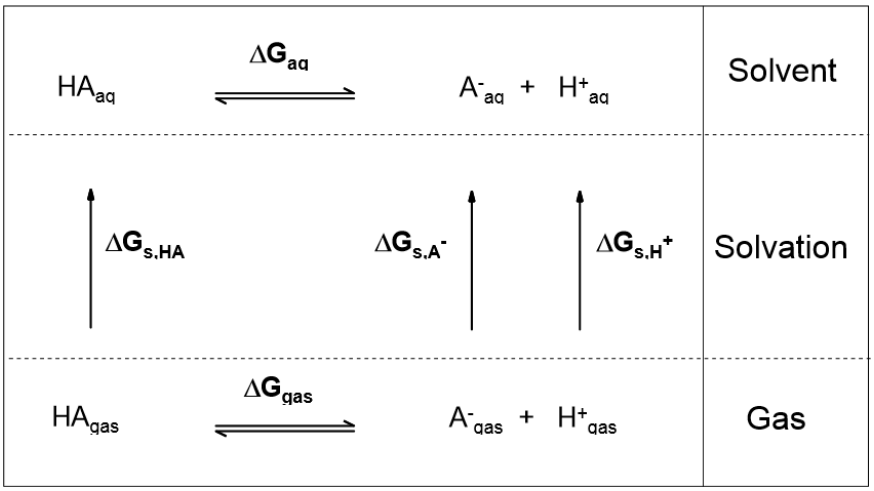

Figure 5.1: Thermodynamic Cycle - The denominator "g" refers to the gas phase and "aq" refers to the condensed phase in water

Due to the gas phase possessing a standard state of 1 atm, while the solvation possesses 1 mol/L, all gas phase energies have to be transferred to the latter state by adding RT*ln(24.46). By applying equation 5.7 to the thermodynamic cycle shown in Figure 5.1 one obtains:

$$\begin{aligned} \Delta G_{aq} = G_{gas}(A^-) + \Delta G_s(A^-) \\ +G_{gas}(H^+) + \Delta G_s(H^+) \\ -G_{gas}(HA) - \Delta G_s(HA) \end{aligned} \tag{5.8}$$

Note: as the accurate calculation of a proton in solvation is not achievable for the approaches used in this work, literature values have been taken: -265.9 kcal/mol for $\Delta G_s^{298}(H^+)$ and -6.28 kcal/mol for $G_{gas}(H^+)$.[34][35]

A recent work by Junming Ho tested whether a thermodynamic cycle using SMD is an improvement when compared to a direct optimization-frequency calculation with this solvation model (see equation [26]). The results showed that for the majority of calculations, both approaches gave similar results (about 0.4 pK$_a$ units difference). However, for cases in which the solvent phase and gas phase geometries were significantly different, the direct calculation was an improvement over the thermodynamic cycle. The direct calculation approach was thus included in this thesis. To give an example, the direct calculation of the hydrogen abstraction by CIP is expressed as shown in equation 5.9:

$$\Delta G_{aq} = G_{aq}^{298}(A^-) - G_{aq}^{298}(HA) + \Delta G_s^{298,lit}(H^+) + G_{gas}^{298,lit}(H^+] \tag{5.9}$$

5.2.2 Protocols for pK$_a$ Calculation

While equation 1.5 holds true for all pK_a computations using the Haber-Born cycle, there are variations to the definition of ΔG_s. To clarify these variations, it is important to establish a nomenclature, as well as a set of definitions for parameters:

- E: refers to the electronic energy of a compound. In Gaussian09, it is equal to "HF" - assuming no counterpoise correction is used.

- G: refers to the Gibbs free energy. In Gaussian09, it is equal to the "sum of electronic and thermal Free Energies"

- G^{corr}: refers to the thermal correction of the free energy. In Gaussian09, it is equal to "thermal correction to Gibbs free energy"

- G_{nes}: refers to the non-electrostatic energy contribution, which is not explicitely taken into account as it is implicit in SMD
- $_{gas/aq}$: refers to a type of calculation: "gas" to a gas phase calculation and "aq" refers to a condensed phase calculation
- (g/l): refers to the geometry used for the calculation: "g" to a gas phase optimized geometry, "l" refers to a condensed phase optimized geometry

Thus, $G_{aq}(l)$ refers to a condensed phase calculation based on a geometry optimization in solution.

Three protocols are used in this work. These approaches differ by the definition of a compound's Gibbs free energy of solvation (ΔG_s):

a) Unrelaxed Solvation

$$\Delta G_s = E_{aq}(g) - E_{gas}(g) + G_{nes,aq}(g) \tag{5.10}$$

b) Relaxed Solvation

$$\Delta G_s = E_{aq}(l) - E_{gas}(g) + G_{nes,aq}(l) \tag{5.11}$$

By combining equation 5.6 and equation5.7 we obtain:

$$\begin{aligned} \Delta G_{aq} = G_{gas}(A^-) + G_{gas}(H^+) - G_{gas}(HA) + \\ \Delta G_s(A^-) + \Delta G_s(H^+) - \Delta G_s(HA) \end{aligned} \tag{5.12}$$

It is important to note, that each separate compound using gas phase energies (including the mentioned gas phase literature values) needs to be corrected by RT*ln(24,46) to account for the difference of units between gas phase (1 atm) and condensed phase (1 mol). As an example, in the case of Relaxed Solvation equation 5.12 becomes:

$$\begin{aligned} \Delta G_{aq} = G_{gas}(g)(A^-) + E_{aq}(l)(A^-) - E_{gas}(g)(A^-) \\ -G_{gas}(g)(HA) - E_{aq}(l)(HA) + E_{gas}(g)(HA)) \\ +(-6.28 kcal/mol) + (-265.9 kcal/mol) \\ +(2-1) * RT * ln(24,46) \end{aligned} \tag{5.13}$$

The $2 - 1$ in the last row represents the two products and the educt, of which each is corrected by RT*ln(24, 46). It is not only possible to describe a protonation, but also a proton exchange. In this work, both a hydroxide anion (formula 5.14) and a hydronium cation (formula 5.15) have been chosen as optional reaction partners for the acid:

$$HA + HO^- \rightleftharpoons A^- + H_2O \tag{5.14}$$

$$HA + H_2O \rightleftharpoons A^- + H_3O^+ \tag{5.15}$$

Again, ΔG_{aq} will be described by the energy difference of products and educts, which is

$$\Delta G_{aq} = G_{aq}(A^-) + G_{aq}(H_2O) - G_{aq}(HA) - G_{aq}(HO^-) \tag{5.16}$$

for the reaction from hydroxide to water and

$$\Delta G_{aq} = G_{aq}(A^-) + G_{aq}(H_2O) - G_{aq}(HA) - G_{aq}(HO^-) \tag{5.17}$$

for the reaction from water to hydronium. However, in these cases one substance is deprotonated while the other is protonated. Therefore ΔG_{aq} corresponds to the difference in the acid dissociation constant and the pK_a of the protonated product has to be added after applying equation 5.5. The pK_a of water and the hydronium are 14 and 0, respectively. We can use the same approach for the proton exchange reaction shown in equation 5.16 , equation 5.7 and the definition of the Relaxed Solvation:

$$\begin{aligned} \Delta G_{aq} = {} & G_{gas}(g)(A^-) + E_{aq}(l)(A^-) - E_{gas}(g)(A^-) \\ & + G_{gas}(g)(H_2O) + E_{aq}(l)(H_2O) - E_{gas}(g)(H_2O) \\ & - G_{gas}(g)(HA) - E_{aq}(l)(HA) + E_{gas}(g)(HA) \\ & - G_{gas}(g)(HO^-) - E_{aq}(l)(HO^-) + E_{gas}(g)(HO^-) \end{aligned} \tag{5.18}$$

Please note that in the case of equation 5.18 the gas phase corrections cancel each other. Reference values are only taken for ΔG_s of HO^-, H_2O and H_3O^+ which are -104.6, -6.32 and -110.4 kcal/mol, respectively.[36][37][38] In this thesis, equations 5.13 and 5.18 are used for the calculation of the pK_a.

5.3 Calculation of pK_a^*: the Förster cycle

The Förster cycle is an approach to predict excited state acid dissociation constants (pK_a*). In the case of a general acid dissociation reaction the Förster cycle is defined as depicted in Figure 5.2. The absorption/emission band corresponding to the acid dissociation will be shifted between the acid (HA) and its conjugated base(A^-). It thus corresponds to the changes of the standard enthalpy in ground and excited state (ΔH and $\Delta H*$, respectively) as follows:

$$N_A hc\nu_{HA} + \Delta H* = N_A hc\nu_{A^-} + \Delta H \tag{5.19}$$

Where N_A is the Avogadro constant, which has to be used as ΔH and ΔH^* are molar quantities whereas absorption/emission bands are not.

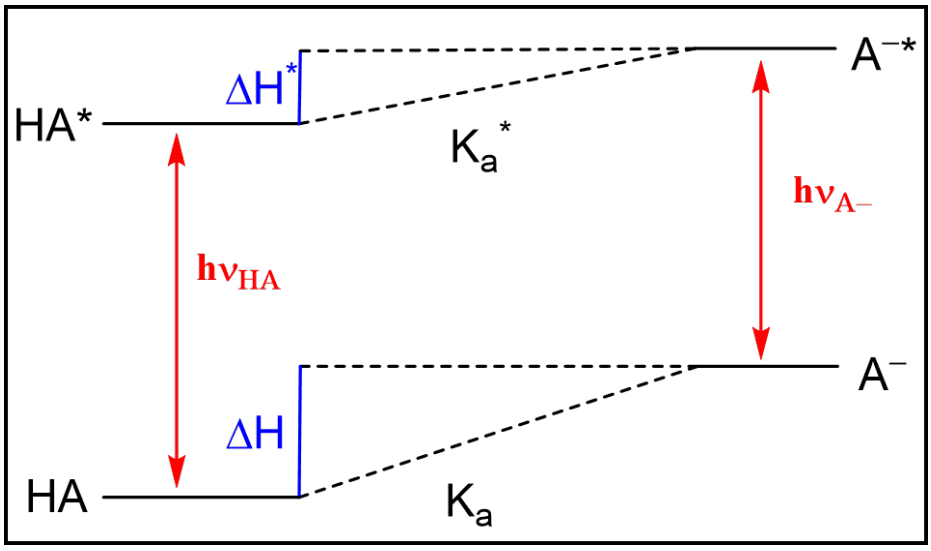

Figure 5.2: The protolytic Förster Cycle for the reaction $HA \rightarrow H^+ + A^-$.

Assuming that the entropy is the same for both reactions, the difference of the ground and excited state standard enthalpy of the dissociation reaction is directly correlated to the difference between the respective acid dissociation constants as described in equation 5.20:

$$\Delta pK_a = pK_a* - pK_a = \frac{\Delta H* - \Delta H}{RTln(10)} \tag{5.20}$$

By combining formula 5.19 and 5.20 one can correlate the shift of the absorption/emission bands to ΔpK_a:

$$\Delta pK_a = \frac{N_A hc(\nu_{A^-} - \nu_{HA})}{RTln(10)} \tag{5.21}$$

It is notable that this equation is valid up to a temperature of 300 K.[39]

6 Results and Discussion

6.1 Acid Dissociation Constants

This section discusses the results regarding the calculated acid dissociation constants of 2-naphtol, 4-nitrophenol and ciprofloxacin.

6.1.1 Benchmark Calculations

One of the first steps within the workflow considered the use of three solvent moldes: PCM, CPCM and SMD. Table 6.1 shows that PCM and CPCM perform in a similar fashion. While none of the calculated acid dissociation constants achieved chemical accuracy, SMD is by 2.5 units closer to the experimental value than the other solvent models. Furthermore, the addition of a zero-point energy correction does not seem to improve the results. It was thus disregarded in all further calculations.

Table 6.1: Comparison of different solvent models with regard to the pK_a of 2-naphthol using M06-2X/aug-cc-pVTZ. pK_a-calculations employed the Born-Haber cycle.

2N: pK_a-Comparison of CSMs (BH)				
Solvation	*CPCM*	*PCM*	*SMD*	*Experiment*
no ZPE-Corr.	14.95	14.98	12.43	9.5
ZPE-Corr.	15.13	15.16	12.61	

Using SMD, several DFT methods were tested with regard to the calculation of ground and excited state acid dissociation constants (see Figure 6.1.1). The excited state pK_a was calculated by applying the Förster cycle with the average of the absorption and emission band energies calculated via linear response. The two best ground state pK_as were obtained by BMK and CAM-B3LYP. The $pK_a{}^*$ was

estimated best by APFD and CAM-B3LYP (see Figure 6.1.1). It is notable that the use of the double-ζ Pople basis set instead of aug-cc-pVTZ improves the values by a great margin.

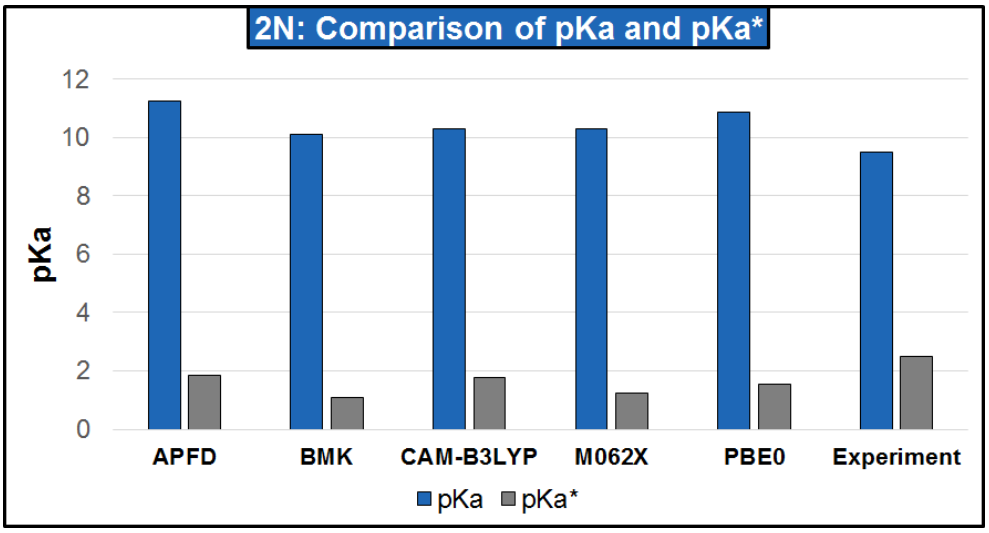

Figure 6.1: Comparison of 2-naphthol's ground and excited state pK_a values calculated by various DFT methods using 6-311+G(d)/SMD.

Table 6.2: ΔpK_a^* of 2N using the emission energy.

Method	**pK_a**	$\Delta pK_a^*{}_{Em}$			$pK_a^*{}_{Em}$		
		LR	**cLR**	**SS**	**LR**	**cLR**	**SS**
APFD	11.23	-8.37	-13.63	-10.31	2.87	-2.40	0.92
BMK	10.11	-7.91	-7.94	-9.39	2.20	2.17	0.72
CAM-B3LYP	10.29	-7.48	-11.98	-8.78	2.82	-1.69	1.51
M062X	10.31	-8.13	-12.62	-9.61	2.18	-2.30	0.71
PBE0	10.86	-8.30	-13.51	-10.23	2.56	-2.65	0.63
Experimental	9.5	-6.1 to -7.0			2.5 to 3.4		

Table 6.3: Calculation of ΔpK_a^* of 2N using the absorption energy.

Method	pK_a	ΔpK_a^* Abs			pK_a^* Abs		
		LR	**cLR**	**SS**	**LR**	**cLR**	**SS**
APFD	11.23	-10.36	-13.97	-6.69	0.87	-2.73	4.54
BMK	10.11	-10.15	-13.39	-6.35	-0.04	-3.29	3.75
CAM-B3LYP	10.29	-9.57	-12.81	-5.50	0.73	-2.52	4.79
M062X	10.31	-10.03	-13.35	-6.07	0.28	-3.03	4.24
PBE0	10.86	-10.37	-13.94	-6.70	0.50	-3.08	4.16
Experimental	9.5	-6.1 to -7.0			2.5 to 3.4		

Tables 6.2, 6.3 and 6.5 apply the Förster cycle using linear response (LR), corrected linear response(cLR) and the state-specific approach (SS).

For 2-naphthol, the change of the acid dissociation constant calculated by the linear response approach using the emission bands seems to provide better results than the two alternatives (see Tables 6.2). Among the methods, BMK and CAM-B3LYP performed best considering the prediction of the shifts. APFD and CAM-B3LYP calculated excited state pK_as which compliment the experimental values.

For the absorption bands (Table 6.3), the state-specific formalism seems to be more accurate than the alternatives. The acidity shifts predicted by APFD, BMK and PBE0 fit the experimental values, whereas the pK_a^* is predicted best by BMK. However, none of the calculated acid dissociation constants are in line with the experiment. While the SS approach using absorption bands predicts the pK_a shift better than the combination of emission bands and linear response, its resulting pK_a^* is less accurate.

Table 6.4: Comparison of ground state pK_a values of 4NP calculated by various DFT methods using 6-311+G(d)/SMD. 'D' stands for the direct use of Gibbs free energies, 'BH' denotes the use of the Born-Haber cycle.

4NP: pK_a-Comparison of Methods				
Method	*APFD*	*BMK*	*CAM-B3LYP*	*Experiment*
BH	5.25	3.46	4.54	7.15
D	5.16	3.25	4.38	

4-nitrophenol proves to be challenging to our approach, as none of the methods in Table 6.4 are within one pK_a unit of the experimental value.

Table 6.5: Comparison of pK_a shifts of 4NP, calculated using CAM-B3LYP/6-311+G(d).

Method	$\Delta pK_a{}^*{}_{Em}$			$\Delta pK_a{}^*{}_{Abs}$		
	LR	**cLR**	**SS**	**LR**	**cLR**	**SS**
APFD	30.29	40.76	71.43	-7.57	-10.27	-1.95
BMK	—	4.42	3.54	-7.19	-1.88	-4.34
CAM-B3LYP	—	9.82	8.65	-9.99	-5.49	-7.29

Mimicking the elimination steps of the workflow, the three approaches using APFD, BMK and CAM-B3LYP were tested with 4-nitrophenol (see Table 6.5). While no experimental excited state acid dissociation constant is available, the differences among the results of an approach speak for its reliability. Surprisingly, the state specific approach was the least consistent among all, with a positive shift of 34.74 pK_a units for the average of absorption and emission bands , but -1.95 for just the absorption.
The linear response might not show the best results, but the shifts appear to be comparatively consistent among all tested methods, granted one employs only the absorption band for calculation.

Table 6.6: Comparison of pK_a values of 2N depending on the Pople basis set. 'D' denotes the direct use of Gibbs free energies,'BH' indicates the employment of the Born-Haber cycle. Calculations were performed with CAM-B3LYP/SMD.

2N: Influence of the Basis Set					
Comparison	Basis Set	$pK_{a,D}$	$\Delta pK_{a,D}$	$pK_{a,BH}$	$\Delta pK_{a,BH}$
6-31 / 6-311	6-31+G(d)	11.24	-0.68	10.85	-0.56
	6-311+G(d)	10.57		10.29	
	6-31+G(d,p)	13.48	-0.17	13.37	-0.42
	6-311+G(d,p)	13.30		12.95	
(d) / (d,p)	6-31+G(d)	11.24	2.23	10.85	2.52
	6-31+G(d,p)	13.48		13.37	
	6-311+G(d)	10.57	2.74	10.29	2.65
	6-311+G(d,p)	13.30		12.95	
+ / ++	6-31+G(d)	11.24	0.06	10.85	0.00
	6-31++G(d)	11.31		10.85	
	6-311+G(d)	10.57	0.10	10.29	-0.12
	6-311++G(d)	10.66		10.18	
Experiment		9.5			

The comparison of several Pople basis sets (see Table 6.6) showed that the influence of a second diffuse function is barely significant for pK_a-calculations. The addition of a (p)-polarization function simply increases the acid dissociation constant by roughly 2.5 units, rather than increasing the accuracy. Only the increase of the number of basis functions seems to present a reliable and significant improvement. As this work strives to find an approach for comparatively bigger systems, calculations with quadruple-ζ basis set have not been conducted. The method/basis set of our choice is thus CAM-B3LYP/6-311+G(d).

6.1.2 pK_a Calculation of Ciprofloxacin

This section discusses the results concerning the acid dissociation constants of ciprofloxacin and by extension its protonation pathway.

Table 6.7: Compilation of the energy difference in [kJ/mol], the resulting tautomeric constant and relative occurence based on the Gibbs free energy. Calculations were performed on several CIP tautomers with CAM-B3LYP/6-311+G(d)/SMD.

Protonation State	**Tautomers**	ΔG	**Log($K_{t(\Delta G_{smd})}$)**	**rel. Occ. [%]**
Dication	$CipH_3^{2+}{}_{(N4',N1',OH)}$	0.00	0.00	100.0
	$CipH_3^{2+}{}_{(N4',N1,OH)}$	145.20	-25.44	0.0
	$CipH_3^{2+}{}_{(N1',N1,OH)}$	209.21	-36.65	0.0
Cation	$CipH_2^{+}{}_{(N4',OH)}$	0.00	0.00	100.0
	$CipH_2^{+}{}_{(N4',N1')}$	70.77	-12.40	0.0
Neutral	$CipH_{(N4')}$	0.45	-0.08	45.4
	$CipH_{(OH)}$	0.00	0.00	54.6

Table 6.8: Compilation of the energy difference in [kJ/mol], the resulting tautomeric constant and relative occurence based on G_{aq}(Born-Haber cycle). Calculations were performed on CIP tautomers with CAM-B3LYP/6-311+G(d)/SMD.

Protonation State	**Tautomers**	ΔG_{BH}	**Log($K_{t(\Delta G_{smd})}$)**	**rel. Occ. [%]**
Dication	$CipH_3^{2+}{}_{(N4',N1',OH)}$	0.00	0.00	100.0
	$CipH_3^{2+}{}_{(N4',N1,OH)}$	151.57	-26.55	0.0
	$CipH_3^{2+}{}_{(N1',N1,OH)}$	205.90	-36.07	0.0
Cation	$CipH_2^{+}{}_{(N4',OH)}$	0.00	0.00	100.0
	$CipH_2^{+}{}_{(N4',N1')}$	55.67	-9.75	0.0
Neutral	$CipH_{(N4')}$	0.00	0.00	99.3
	$CipH_{(OH)}$	12.28	-2.15	0.7

To create unambiguous results, the fully protonated form, $CipH_4^{3+}{}_{(N4',N1',N1,OH)}$

will be deprotonated on three locations, with the exception of the carbon acid which can be reasonably excluded at low pH. Tables 6.7 and 6.8 show that among the three resulting cations, those with a protonated N1 position are by at least 140 kJ/mol less favoured than the unprotonated ones. It is thus safe to conclude that the N1 position of less positively charged forms of CIP remains unprotonated. Furthermore, it seems that the deprotonation at N1′ is preferred by about 50-60 kJ/mol compared to the N4′ position. The next step is the removal of a hydrogen from the energetically favoured dication $CipH_3^{2+}{}_{(N4',N1',OH)}$. As N1 does not possess a hydrogen anymore and a protonated N4′ is quite stable, the deprotonations of N1′ and OH had to be compared.

Table 6.9: List of ciprofloxacins micro-pK_as calculated using CAM-B3LYP/6-311+G(d).

Educt	**Product**	**Label**	**D: Micro-pK_a**	**BH: Micro-pK_a**
$CipH_4^{3+}{}_{(N4',N1',N1,OH)}$	$CipH_3^{2+}{}_{(N4',N1',OH)}$	$pK_{a,m1}$	-34.90	-34.63
	$CipH_3^{2+}{}_{(N4',N1,OH)}$	- - -	-9.46	-8.07
	$CipH_3^{2+}{}_{(N1',N1,OH)}$	- - -	1.75	1.45
$CipH_3^{2+}{}_{(N4',N1',OH)}$	$CipH_2^{+}{}_{(N4',OH)}$	$pK_{a,m2}$	-7.84	-5.73
	$CipH_2^{+}{}_{(N4',N1')}$	- - -	4.56	4.02
$CipH_3^{2+}{}_{(N4',N1,OH)}$	$CipH_2^{+}{}_{(N4',OH)}$	- - -	-33.28	-32.29
	$CipH_2^{+}{}_{(N4',N1')}$	- - -	-20.88	-22.53
$CipH_3^{2+}{}_{(N1',N1,OH)}$	$CipH_2^{+}{}_{(N4',OH)}$	- - -	-44.49	-41.80
	$CipH_2^{+}{}_{(N4',N1')}$	- - -	-32.09	-32.05
$CipH_2^{+}{}_{(N4',OH)}$	$CipH_{(N4')}$	$pK_{a,m3-2}$	7.02	5.32
	$CipH_{(OH)}$	$pK_{a,m3-1}$	6.94	7.47
$CipH_2^{+}{}_{(N4',N1')}$	$CipH_{(N4')}$	- - -	-5.38	-4.44
	$CipH_{(OH)}$	- - -	-5.46	-2.29
$CipH_{(N4')}$	$CipH^{-}$	$pK_{a,m4-2}$	7.26	7.77
$CipH_{(OH)}$	$CipH^{-}$	$pK_{a,m4-1}$	7.34	5.62

Similar to N4', the protonated carboxylic acid is preferred by roughly 50-70 kJ/mol, thus the most stable cationic tautomere is $CipH_{2\ (N4',OH)}^{+}$. In the case of the direct calculation, the removal of a hydrogen from the cation yields the almost equally stable neutral and zwitterionic tautomers of CIP, with the neutral form being preferred. The Born-Haber cycle predicts the zwitterionic form to be more stable by about 12 kJ/mol.
Several different protonation pathways of fluoroquinolones have been published in literature - most of them are shown in Figure 6.3.

The micro-pK_a of all protonation states has been calculated using the relaxed solvation as discussed in the chapter 'pK_a-Calculation'. Furthermore the tautomeric constant, K_t, was computed by applying the following formula:

$$K_t = e^{-\frac{\Delta G}{RT}} \tag{6.1}$$

where R is the universal gas constant, T is the temperature (in our case $298,15$ K). Depending on whether the direct approach or the Born-Haber cycle was used, ΔG equals the difference of the Gibbs free energy or ΔG_{aq} between two tautomers. The reason for considering the application of the Born-Haber cycle for tautomeric constants is rather simple: Let us assume a compound may deprotonate two ways, resulting in the tautomers A and B. The difference in the micro-pK_a of compound A and B is directly correlated to their difference in their energy in the solvent phase, as is their tautomeric constant. Thus, the micro-pK_a and the tautomeric constant also correlate to each other. If one were to apply the Born-Haber cycle to the micro-pK_a but not to the tautomeric constant, then one would not fit to the other.

Both the direct calculations from the Gibbs free energies and the application of a thermodynamic cycle point towards the same protonation pathway (see Figure 6.2). This pathway is in line with the protonation pathway suggested by Rusu et al. (depicted in Figure 6.3) - aside from the trication, which has not been measured in the work of this group.

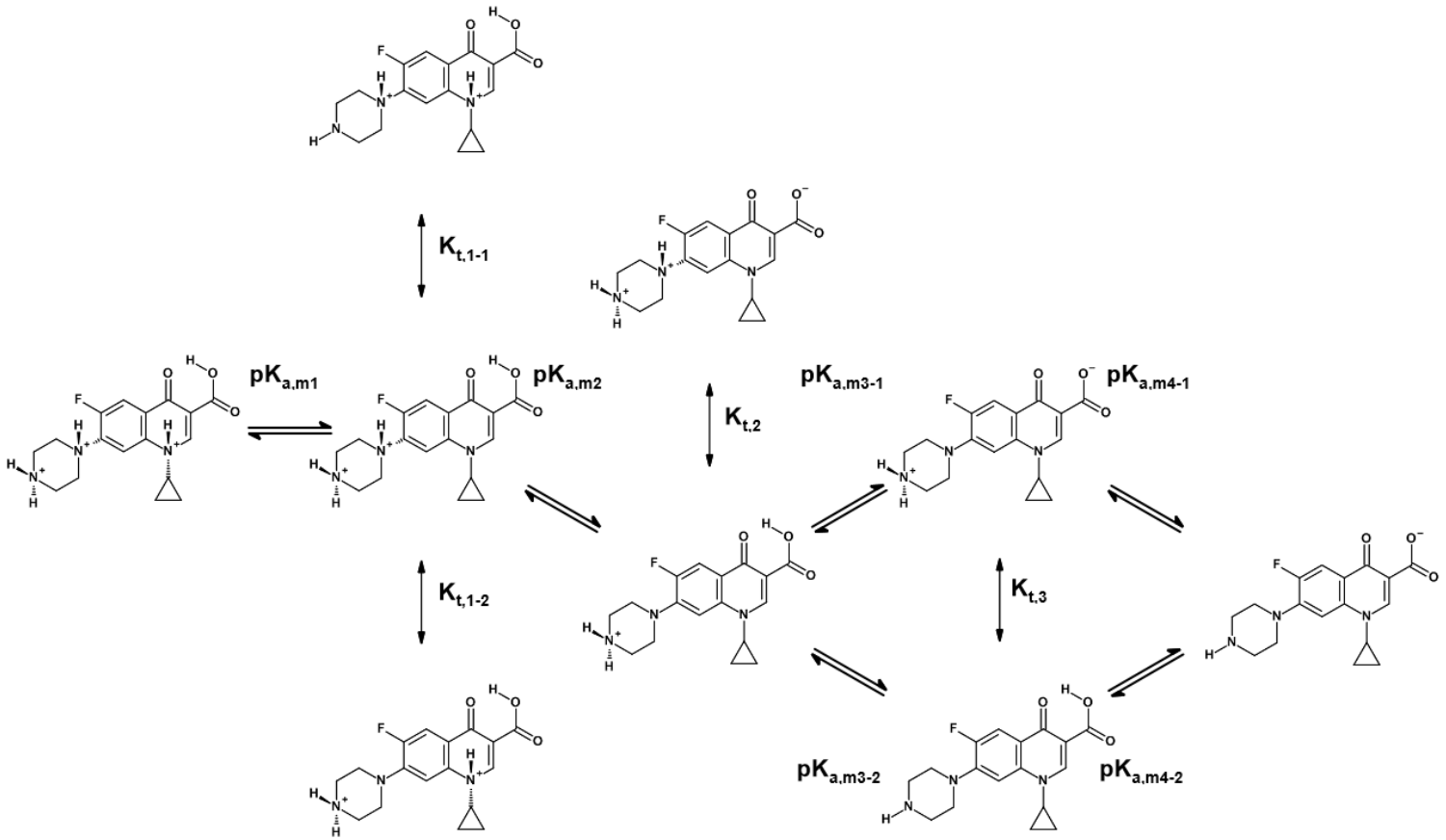

	$pK_{a,1}$		$pK_{a,2}$		$pK_{a,3}$		$pK_{a,4}$		Macro
$ClPH_43+$	⇌	$ClPH_32+$	⇌	$ClPH_2+$	⇌	ClPH	⇌	ClP^-	$-pK_as$

Figure 6.2: Protonation pathway of Ciprofloxacin

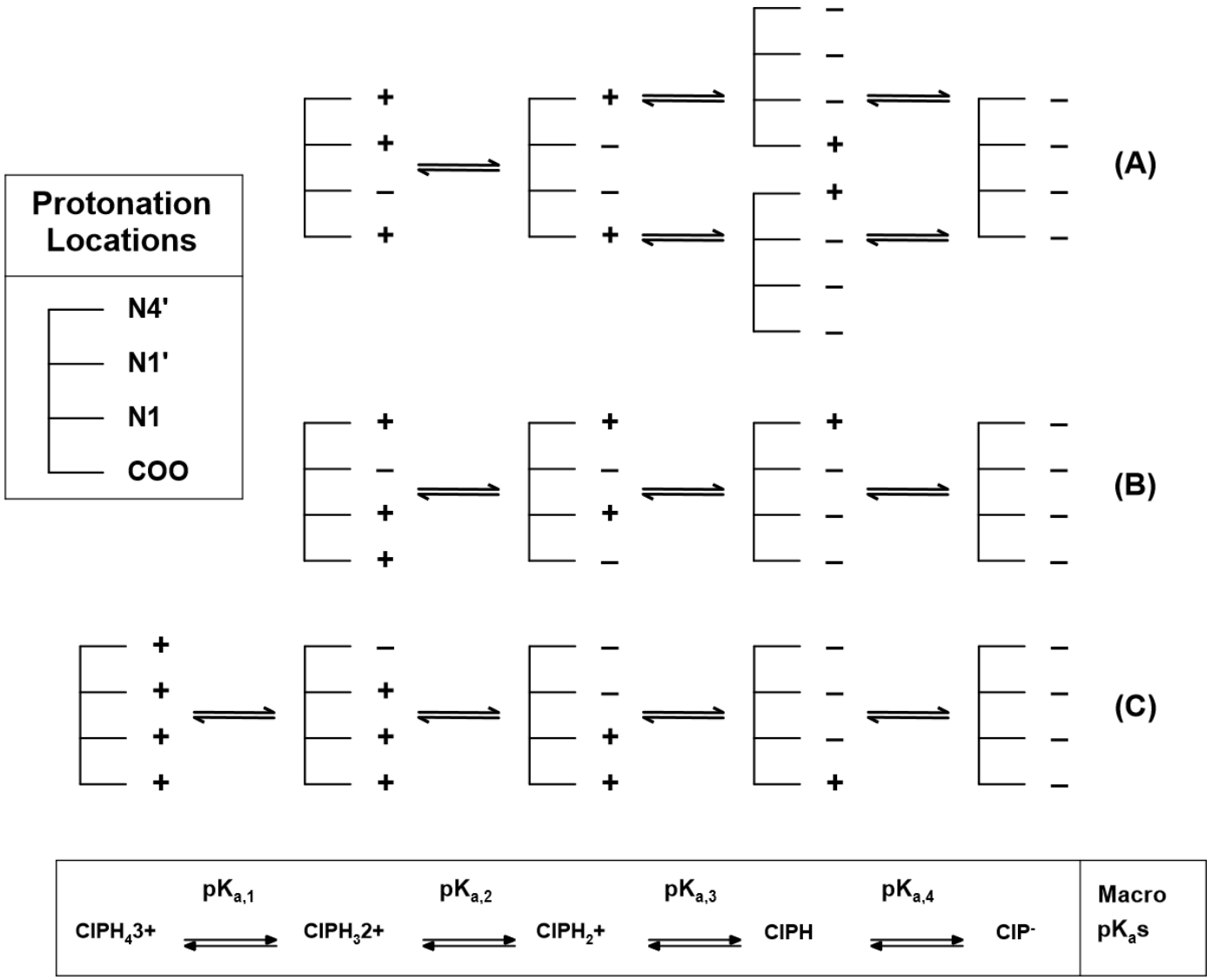

Figure 6.3: Protonation pathways suggested by the following literature:
(A) A. Rusu et al. [40], (B) D. A. Buckingham et. al.[41] and (C) C. Adams and Z. Quiang.[42]

In addition to the deprotonation resulting in a proton and the conjugated base, we considered the proton transfer to a hydroxide and a water molecule (Tables 6.10 and 6.11, respectively. Overall, the reaction with water shows slightly higher pK_a values than the reaction with hydroxide. When compared to the results in Table 6.9, the pK_a of the water and hydroxide reactions are about 2 units higher and therefore deviate more from the majority of literature values than the reaction involving the proton.

Table 6.10: pK_a calculation with the reaction $HA + HO^- \rightarrow A^- + H_2O$ using CAM-B3LYP/6-311+G(d)/SMD.

Product	Educt	Label (Fig. 6.4)	D: Micro-pK_a	BH: Micro-pK_a
$CipH_3^{2+}{}_{(N4',N1',OH)}$	$CipH_4^{3+}{}_{(N4',N1',N1,OH)}$	$pK_{a,m1}$	-32.81	-32.53
$CipH_3^{2+}{}_{(N4',N1,OH)}$		—	-7.37	-5.98
$CipH_3^{2+}{}_{(N1',N1,OH)}$		—	-159.38	-159.96
$CipH_2^{+}{}_{(N4',OH)}$	$CipH_3^{2+}{}_{(N4',N1',OH)}$	$pK_{a,m2}$	-5.74	-3.64
$CipH_2^{+}{}_{(N4',N1)}$		—	6.65	6.11
$CipH_{(N4')}$	$CipH_2^{+}{}_{(N4',OH)}$	$pK_{a,m3-2}$	9.12	7.41
$CipH_{(OH)}$		$pK_{a,m3-1}$	9.04	9.56
Cip^-	$CipH_{(N4')}$	$pK_{a,m4-2}$	9.36	9.86
Cip^-	$CipH_{(OH)}$	$pK_{a,m4-1}$	9.44	7.71

Table 6.11: pK_a calculation with the reaction $HA + H_2O \rightarrow A^- + H_3O^+$ using CAM-B3LYP/6-311+G(d)/SMD.

Product	Educt	Label (Fig. 6.4)	D: Micro-pK_a	BH: Micro-pK_a
$CipH_3^{2+}{}_{(N4',N1',OH)}$	$CipH_4^{3+}{}_{(N4',N1',N1,OH)}$	$pK_{a,m1}$	-32.42	-32.14
$CipH_3^{2+}{}_{(N4',N1,OH)}$		—	-6.98	-5.58
$CipH_3^{2+}{}_{(N1',N1,OH)}$		—	-158.98	-159.56
$CipH_2^{+}{}_{(N4',OH)}$	$CipH_3^{2+}{}_{(N4',N1',OH)}$	$pK_{a,m2}$	-5.35	-3.25
$CipH_2^{+}{}_{(N4',N1)}$		—	7.05	6.51
$CipH_{(N4')}$	$CipH_2^{+}{}_{(N4',OH)}$	$pK_{a,m3-2}$	9.51	7.80
$CipH_{(OH)}$		$pK_{a,m3-1}$	9.43	9.95
Cip^-	$CipH_{(N4')}$	$pK_{a,m4-2}$	9.75	10.26
Cip^-	$CipH_{(OH)}$	$pK_{a,m4-1}$	9.83	8.11

Using CAM-B3LYP/6-311+G(d), both the linear response and the corrected linear response have been tested for their consistency. Results are shown in Tables 6.12 and 6.13. All approaches employing emission bands seem to yield both positive and negative shifts within the same protonation state. Linear response using only the absorption band provides positive shifts for the deprotonation of the neutral forms and negative shifts for the deprotonation of cationic forms.

Table 6.12: Predicted shift of CIP's acid dissociation constant upon excitation according to LR. The used approach was CAM-B3LYP/6-311+G(d)/SMD.

Deprotonated	**Protonated**	$\Delta\mathbf{pK}_{a^*Em}$	$\Delta\mathbf{pK}_{a^*Abs}$	$\Delta\mathbf{pK}_{a^*Em}$
Anion oH	*Neutral oH*	1.76	1.58	1.94
Anion oH	*Zwitter oH*	-3.30	0.32	-6.92
Neutral oH	*Cation oK*	-2.33	-1.60	-3.05
Zwitter oH	*Cation oK*	2.74	-0.33	5.81

Table 6.13: Predicted shift of CIP's acid dissociation constant upon excitation according to cLR. The used approach was CAM-B3LYP/6-311+G(d)/SMD.

Deprotonated	**Protonated**	$\Delta\mathbf{pK}_{a^*Em}$	$\Delta\mathbf{pK}_{a^*Abs}$	$\Delta\mathbf{pK}_{a^*Em}$
Anion oH	*Neutral oH*	0.72	-2.63	4.07
Anion oH	*Zwitter oH*	-2.58	1.29	-6.46
Neutral oH	*Cation oK*	-5.61	-2.22	-9.00
Zwitter oH	*Cation oK*	-2.31	-6.15	1.53

The relaxed solvation protocol was used for the favoured conformations of ciprofloxacin. $pK_{a,m2}$ is vastly more negative for the unrelaxed than the relaxed protocol (-32.02 and -7.84, respectively). While $pK_{a,m4-2}$ and $pK_{a,m3-2}$ are not too far from the experimental values, $pK_{a,m4-1}$ is much smaller than $pK_{a,m3-1}$, rendering the protocol too unreliable.

Table 6.14: pK_a values of CIP calculated using unrelaxed solvation and CAM-B3LYP/6-311+G(d)/SMD.

Product	**Educt**	**Micro-pK_a**	
		Label	*BH - Unrelaxed*
$CipH_{2\ (N4',OH)}^{+}$	$CipH_{3\ (N4',N1',OH)}^{2+}$	$pK_{a,m2}$	-32.02
$CipH_{(N4')}$	$CipH_{2\ (N4',OH)}^{+}$	$pK_{a,m3-2}$	4.97
$CipH_{(OH)}$		$pK_{a,m3-1}$	8.83
Cip^{-}	$CipH_{(N4')}$	$pK_{a,m4-2}$	8.77
Cip^{-}	$CipH_{(OH)}$	$pK_{a,m4-1}$	4.92

It is important to note that the literature is ambiguous regarding experimental acid dissociation constants of Ciprofloxacin, as the results depend on the measuring method - however, the vast majority agrees with the pK_a values at about 8.7 and 6.1. We did not find any literature which claims to have measured the $pK_{a,1}$, the acid dissociation constant of the trication. Table 6.15 shows three of those measurements and compares them with our best result and assignment:

Table 6.15: Some literature values of the pK_as of CIP

Cip: Comparison of pK_a			
Approach	pK_a, 4	pK_a, 3	pK_a, 2
1H NMR Titration [40]	8.61	6.30	-0.21
Potentiometr. Titration [42]	10.58	8.70	6.41
Microch. Electrophoresis [43]	8.95	6.35	5.05
Best approach in this work	7.34	6.94	-7.84

6.2 UV-Vis Results

This section contains the results concerning the predicted UV-Vis spectra, the individual transitions and the comparisons of these spectra to the experiments. The description of important transitions includes the discussion of the involved orbitals.

6.2.1 Experimental Spectra

The spectra of CIP are depicted in Figure 6.4.[44] In the left part, acidic spectra are shown and the maxima of the transitions with lower energies are at about 366, 328 ($n \rightarrow \pi^*$), 314 ($n \rightarrow \pi^*$) and 270-275 nm($\pi \rightarrow \pi^*$) - it is important to note that the '$1 \rightarrow 10$' denotes the molarity of the HCl used in the solution.

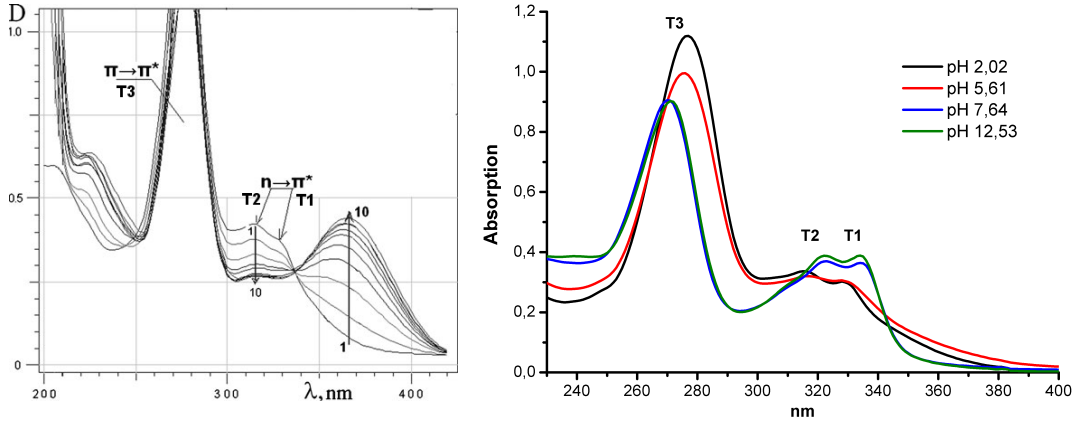

Figure 6.4: Experimental spectra of CIP at pH 0 to −1 (left), obtained by Polishchuk et al. [44], and pH 2.02 to 12.53 (right) measured by M. Montemurro, who kindly provided the spectra for publication in this thesis. [45] T1,2 and 3 denote the 1^{st}, 2^{nd} and 3^{rd} major transition, respectively.

In the right part of Figure 6.4, the experimental spectra provided by M. Montemurro, Laboratorio de Desarrollo Analítico y Quimiometría (UNL) are shown. They are in good agreement with those of Polishchuk et al. - except for the peak at 366 nm which was not observed at a pH above 2.
The lack of this transition indicates that the very acidic environment in Polishchuk's work has given rise to a di- or trication of CIP. For further discussion we will refer to the three most prominent peaks shown in Polishchuk's spectra (Figure 6.4) as major transitions. These peask are at 328, 314 and 272.5 (the average of 270 and 275) nm, and will be denoted as first, second and third major transition, respectively.
When changing from an acidic to a basic pH, the right part of Figure 6.4 shows a

red-shift of all bands above about 310 nm, causing the first major transition to shift from 328 to 335 nm and the second to shift from 314 to 322 nm. Additionally, a blue-shift of bands with smaller wavelengths occurs, with the third major transition changing from about 275 to 270 nm. Beside slight changes of intensities, the spectra recorded at pH 2.02 and 5.61 do not show any significant differences. The same accounts for the spectra of pH 7.64 and 12.53.

6.2.2 Calculated Absorption Spectra of 2N and CIP

Using several DFT methods in combination with SMD and the basis set def2-TZVP, UV-Vis spectra of CIP have been compared to the experimental spectrum of our cooperators (see right part of Figure 6.4). For this task, the geometries optimized with M06-2X/6-31+G(d) have been used. The following section discusses the neutral molecule spectra shown in Figure 6.5 with regard to the experiment. Please note that each method shifts the spectra.

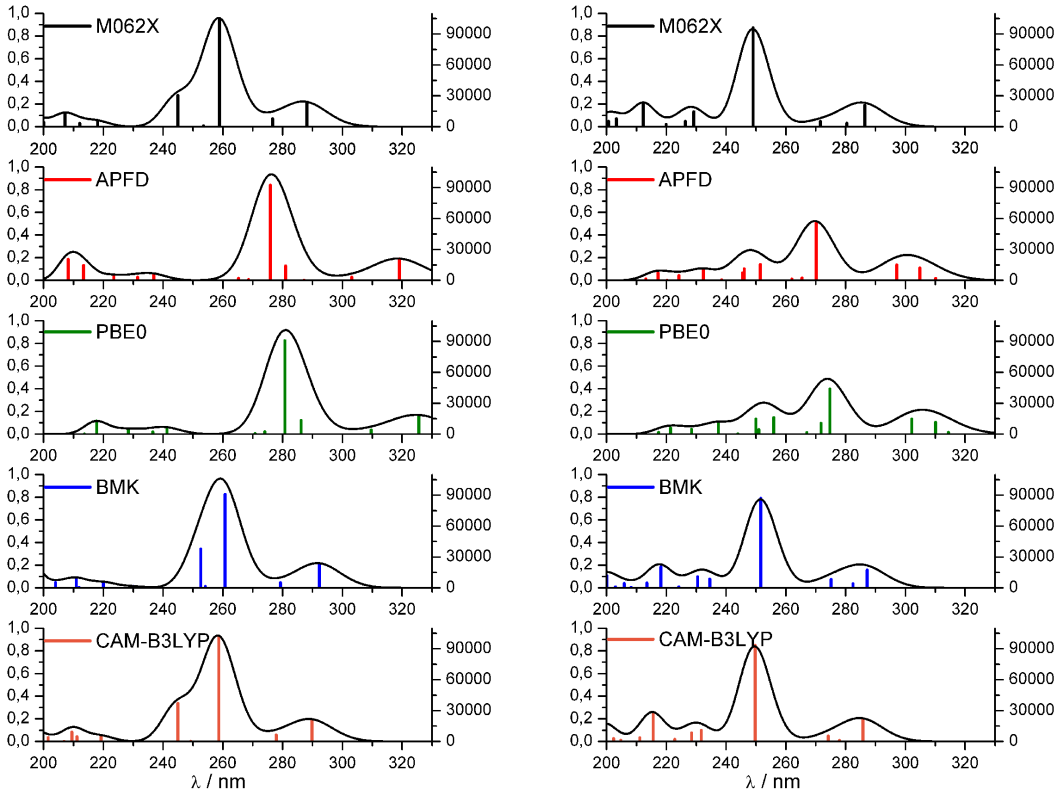

Figure 6.5: Comparison of methods: absorption spectra of the zwitterionic (right) and the neutral form (left) of CIP

For all methods, all major transitions of the zwitterions are blue-shifted compared to their respective neutral form. For the neutral forms, the intensity of the third major transition is greater than the one of the zwitterions. The highest absorption wavelength of the neutral compound seems to correspond to the experimental peak at 328 nm. A similar claim can be made for the 2-3 peaks with the highest wavenumbers of the zwitterion, which seem to correspond to first and second major transitions.

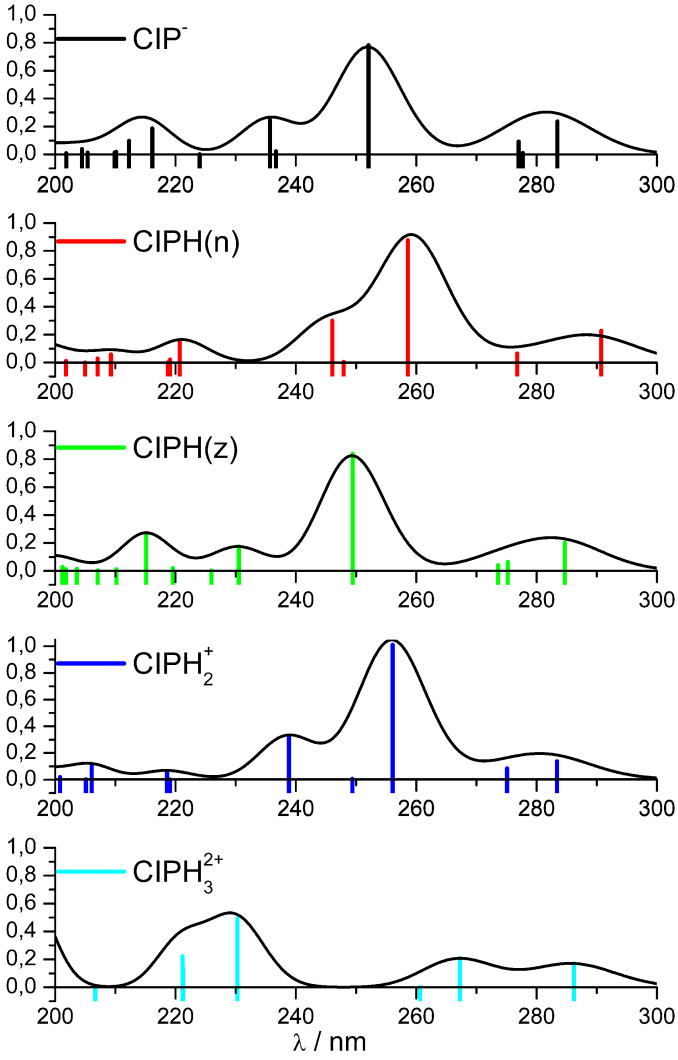

Figure 6.6: Spectra of Ciprofloxacin in different protonation states calculated with CAM-B3LYP/6-311+G(d) and SMD

In experiments, the third major absorption (at 270-275 nm) shows the highest

intensity - this is also true for the corresponding peak of the calculated spectra for all methods and protonation states of CIP. APFD and PBE0 perform quite similar. Both M06-2X and CAM-B3LYP calculate spectra which are akin to those of BMK. The UV-Vis spectra of CIP in different protonation states have been calculated using CAM-B3LYP/6-311+G(d) with SMD (see Figure 6.6). These spectra will be compared to the experimental data depicted in Figure 6.4 which has been provided by our cooperators in Argentina. Compared to this experiment, the calculated spectra of Figure 6.6 are shifted towards smaller wavelengths. Both $n \rightarrow \pi^*$ transitions (major transition 1 and 2, see Figure 6.4) were predicted, altough the one at lower wavelengths tends to lack intensity. Unlike in the experimental spectra, no clear trend among different protonation states - and thus with changing pH value - is observed.

6.2.3 Impact of Conformation on Spectra

As two conformers with different positions of the cyclopropane (0 = above/1 = below the aromatic plane, see Nomenclature) possess similar energies, it was interesting to test whether a significant difference between the spectra of such isomers exists. The spectra of the 0/1 conformers of the zwitterion and the neutral form of CIP can be seen in Figure 6.7. Their wavelengths only differ by about 1 to 2 nm and the variations regarding intensities are small. Thus the influence of such conformational differences is insignificant for the calculation of absorption spectra.

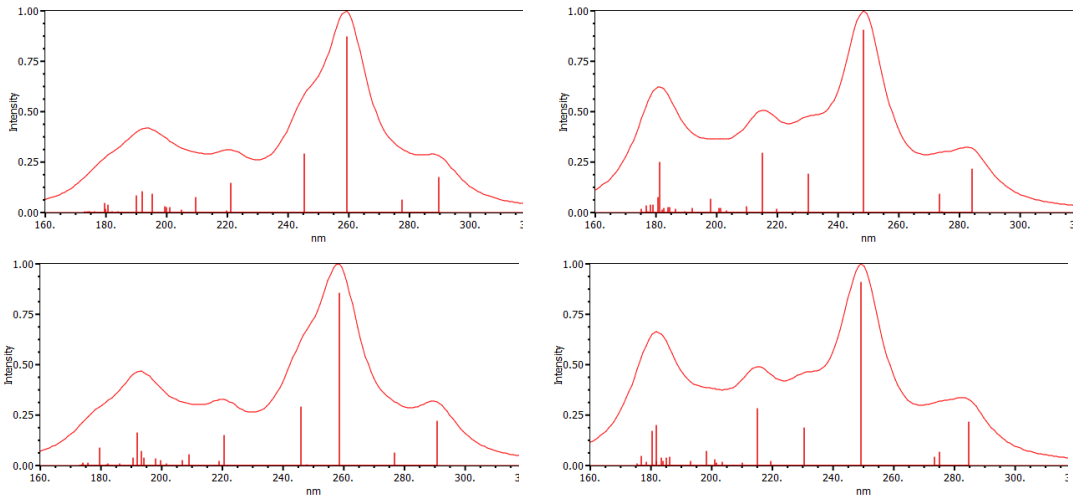

(a) Neutral (CIPH) (b) Zwitterionic (CIPH)

Figure 6.7: Influence of the cyclopropane position (0 - left, 1 - right) on the absorption spectrum calculated using CAM-B3LYP/6-311+G(d)/SMD.

6.2.4 Absorption Band Deviations among DFT Methods

Within this section, all non-experimental wavelengths were calculated using linear response. Taking both Tables 6.16 and 6.17 into account, M06-2X possesses the greatest deviation to the experimental values among all tested functionals. However, BMK and CAM-B3LYP show similar fluctuations. It is notable that M06-2X, BMK and CAM-B3LYP always seem to overestimate the energy gap of these transitions.

Table 6.16: Wavelengths and peak maximum errors of UV-Vis spectra of the neutral form of CIP. Calculated based on the M06-2X/6-31+G(d)/SMD geometry and using def2-TZVP/SMD.

Peak Position in nm					
Exp [nm]	*APFD*	*BMK*	*CAM-B3LYP*	*M06-2X*	*PBE0*
328	319.1	292.3	289.8	288.1	325.6
314	303.1	279.2	277.8	276.6	309.6
272.5	275.9	260.7	258.6	258.9	286.2
Error in eV					
Exp [eV]	*APFD*	*BMK*	*CAM-B3LYP*	*M06-2X*	*PBE0*
3.78	0.11	0.46	0.50	0.52	0.03
3.95	0.14	0.49	0.51	0.53	0.06
4.55	-0.06	0.21	0.24	0.24	-0.22

Table 6.17: Wavelengths and peak maximum errors of UV-Vis spectra of the zwitterionic form of CIP. Calculated based on the M06-2X/6-31+G(d)/SMD geometry and using def2-TZVP/SMD.

Peak Position in nm					
Exp [nm]	*APFD*	*BMK*	*CAM-B3LYP*	*M06-2X*	*PBE0*
328	304.8	287.2	285.8	286.4	310.0
314	297.1	275.2	274.2	271.6	302.1
272.5	270.1	251.6	249.6	249.0	274.7
Error in eV					
Exp. [eV]	*APFD*	*BMK*	*CAM-B3LYP*	*M06-2X*	*PBE0*
3.78	0.29	0.54	0.56	0.55	0.22
3.95	0.22	0.56	0.57	0.62	0.16
4.55	0.04	0.38	0.42	0.43	-0.04

In the case of CAM-B3LYP this is a circumstance that has already been adressed by Jacquemin et al., who describes the average overestimation to be at about 0.26 eV for π-π^* transitions and 0.21 eV for n-π^* transitions.[46]
If the data is corrected by this value, the difference in transition energies of CAM-B3LYP would vary from $+0.23$ to -0.9 eV, thus possessing an error range of 0.32 eV. Please note that error ranges within this section will be displayed in brackets after the lower error deviation, for example: 0.5 to -0.1 eV (0.6 eV), would refer to an error range of 0.6 eV. While PBE0 shows the least overall error, but its deviation ranges from $+0.22$ to -0.22 (0.44 eV), which is inferior to the corrected CAM-B3LYP. APFD shows both a low error and a small divergence, with just $+0.29$ to -0.06 eV (0.35 eV).

Table 6.18: Wavelengths and errors of UV-Vis spectra of four protonation states of CIP. Calculations were based on the M06-2X/6-31+G(d)/SMD geometry and performed using APFD/def2-TZVP/SMD."Experimental" refers to the experimental peak maximum.

	Peak Position in nm			*Error in eV*		
Experimental	**328**	**314**	**272.5**	**3.78**	**3.95**	**4.55**
Anion (CIP^-)	313.2	306.5	273.3	0.18	0.10	-0.01
Neutral (CIPH)	319.1	303.1	275.9	0.11	0.14	-0.06
Zwitter (CIPH)	304.8	297.1	270.1	0.29	0.22	0.04
Cation ($CIPH_2^+$)	305.1	296.2	277.3	0.28	0.24	-0.08

Table 6.19: Wavelengths and errors of UV-Vis spectra of four protonation states of CIP. Geometries and wavelengths were obtained using CAM-B3LYP/6-311+G(d) with SMD."Experimental" refers to the experimental peak maximum.

	Peak Position in nm			*Error in eV*		
Experimental	**328**	**314**	**272.5**	**3.78**	**3.95**	**4.55**
Anion (CIP^-)	283.5	277.7	252.1	0.59	0.52	0.37
Neutral (CIPH)	290.8	276.8	258.6	0.48	0.53	0.24
Zwitter (CIPH)	284.7	275.2	249.4	0.58	0.56	0.42
Cation ($CIPH_2^+$)	283.4	275.1	256.1	0.59	0.56	0.29

As APFD showed the most reliable results, the UV-Vis spectra of several protonation states have been calculated using APFD/def2-TZVP/SMD (see Table 6.18). The

λ_{max}values diverge from $+0.29$ to -0.08 eV (0.37 eV), providing a good estimation overall. A very important aspect of these results are the three following trends:

- the decrease of the first transition's wavelengths with increasing charge of the molecule (except the zwitterionic form)
- the decrease of the second transition's wavelengths with increasing charge of the molecule
- the decrease of the third transition's wavelengths with decreasing charge of the molecule (except the neutral form)

These tendencies are in line with the experimental spectra depicted in the right part of Figure 6.4. Table 6.19 contains the transition energies obtained from calculations with CAM-B3LYP/6-311+G(d)/SMD.

Despite the triple-ζ geometries and a smaller error fluctuation (0.3 eV) , APFD/def2-TZVP still seems to be the better combination of method and basis set, for two reasons: One is the required error correction of CAM-B3LYP - without it, several deviations of CAM-B3LYP are greater than 0.5 eV. The other is the non-systematic behaviour of charge and major transitions. The ability to model such behaviour is required to reproduce the experimental trends, which are necessary for our intends and purposes, such as the use of the Förster cycle.

A final comparison among the basis sets 6-311+G(d) and def2-TZVP using APFD was conducted (see Table 6.20). The basis sets performed very similar, with a maximum difference of 4 nanometers among all calculated wavelengths. For both computations the results for the neutral form of ciprofloxacin does not fit any of the trends observed in the experimental spectra. The strong deviations shown by APFD with regards to the ground state pK_a rendered the method too unreliable for the calculation of this constant. CAM-B3LYP, on the other hand, performed quite well for both the ground and excited state acid dissociation constant.

While the excited state pK_a calculation employed linear response, and thus the same values used by UV-Vis spectroscopy, it is noteworthy that the Förster cycle only uses the relative energy of absorption bands and does not necessarily reflect the ability to correctly predict UV-Vis spectra. In the tests CAM-B3LYP against other DFT-methods, APFD has been shown to be more reliable in the prediction of the absolute energies of absorption bands than APFD.

Conclusively, it is recommended to use CAM-B3LYP for ground and excited state pK_a calculations and APFD for the prediction of absorption spectra. The basis set 6-311+G(d) performed wel for all aforementioned tasks.

Table 6.20: Comparison of the basis sets 6-311+G(d) and def2-TZVP using APFD/SMD regarding the major transitions of CIP. Based on CAM-B3LYP/6-311+G(d)/SMD geometries.

Karlsruhe basis set: def2-TZVP						
	Peak Position in nm			**Error in eV**		
Transition	1	2	3	1	2	3
Experiment	328	314	272.5	3.78	3.95	4.55
Anion (CIP^-)	311.9	298.0	263.9	0.19	0.21	0.15
Neutral (CIPH)	326.8	306.4	275.0	0.01	0.10	-0.04
Zwitter (CIPH)	304.4	297.7	268.5	0.29	0.22	0.07
Cation ($CIPH_2^+$)	307.2	296.4	269.5	0.26	0.24	0.05
RMS $\pm$ *STDEV*				*0.18* $\pm$ *0.11*		
Pople basis set: 6-311**+G(d)**						
	Peak Position in nm			**Error in eV**		
Transition	1	2	3	1	2	3
Experiment	328	314	272.5	3.78	3.95	4.55
Anion (CIP^-)	312.6	297.9	267.9	0.19	0.21	0.08
Neutral (CIPH)	328.6	307.7	275.8	-0.01	0.08	-0.05
Zwitter (CIPH)	304.9	297.9	268.6	0.29	0.21	0.07
Cation ($CIPH_2^+$)	308.5	296.7	271.5	0.24	0.23	0.02
RMS $\pm$ *STDEV*				*0.17* $\pm$ *0.11*		

6.3 MO Interpretation for CIP

This section will compare the orbitals of the different protonation states of ciprofloxacin and link them to the experimental absorption bands shown in the left part of Figure 6.4. The following tables contain data concerning the three most important

absorptions. Molecule orbitals number 83 to 89 of each molecule are depicted in the Appendix.
For the lower orbitals (number 83 to 85) of all protonation states the n-orbitals at the ketone and carbon acid possess big coefficients. The p_z orbitals at the piperazine possess significant coefficients in MO number 86 and 87, not including the dication, as it does not possess coefficients at the piperazidin. Instead, it shifts electron density from the ketone and the protonated oxygen of the carbon acid to the aromatic rings and the fluor atom. The next unoccupied MO (88) possesses a high coefficient at the π-orbital of the ketone and the aromatic ring - this and the following statement is true for all protonation states. Orbital 89 shifts density to the π-orbital of the carbon acid moiety.
As shown in Tables 6.21 and 6.22, the first and second major transition are linear combinations of the same electronic transitions, which are switched between the neutral and the zwitterion but still possess similar energies.

For the anionic, the neutral and the cationic CIP, the first absorption band is a charge transfer from the piperazine to the aromatic ring with the ketone - this involves a transition from MO number 87 to 88 (see Figure 6.8) - thus the first absorption is a $n - \pi^*$ transition for these protonation states. In the case of these three molecules, this transition receives a significant contribution from the excitation of orbital 86 to orbital 89 (or 88, in the case of the anion).

Table 6.21: Comparison of the first major transition

Protonation State	Anion CIP^-	Neutral $CIPH$	Zwitter $CIPH$	Cation $CIPH_2^+$	Dication $CIPH_3^{2+}$
Transition	S1	S1	S1	S1	S1
nm	283.5	290.8	284.7	283.4	286.2
f	0.236	0.229	0.202	0.138	0.172
Prim. Orbitals	87->88	87->88	87->88	87->88	87->88
%	0.589	0.611	0.649	0.598	0.678
Sec. Orbitals	86->88	86->89		86->89	
%	-0.232	-0.232		-0.311	

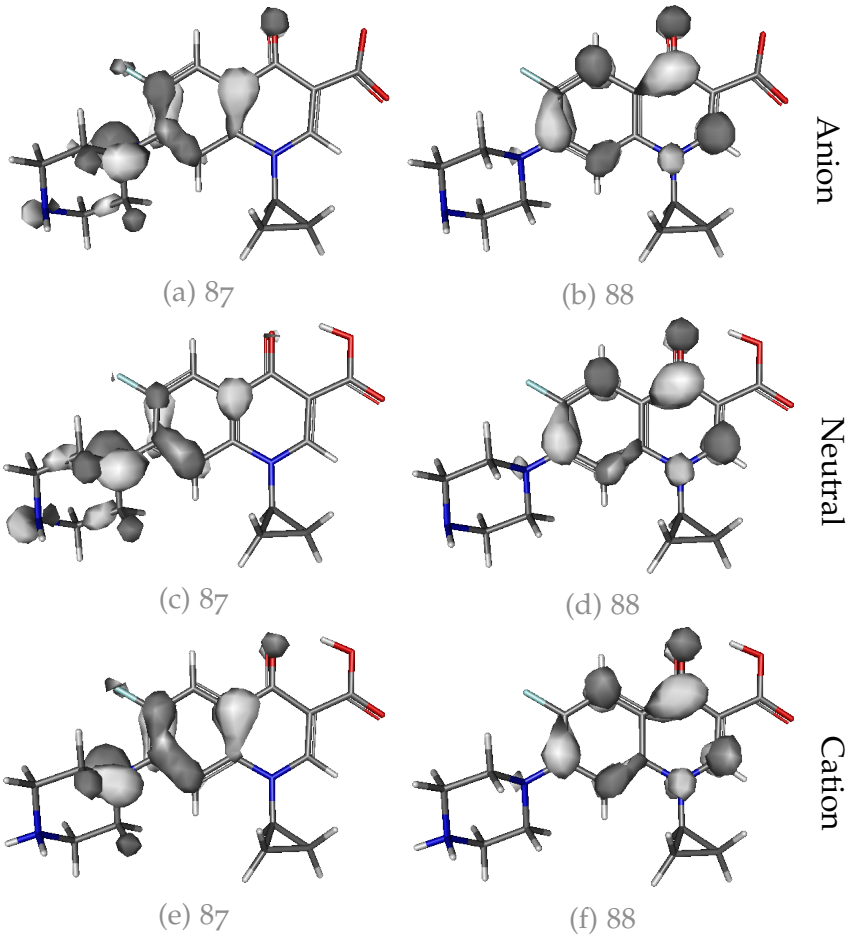

(a) 87 (b) 88

(c) 87 (d) 88

(e) 87 (f) 88

Figure 6.8: 1^{st} major transition: the MOs of the anion, neutral and cation of CIP

The p_z orbitals at the piperazine are part of the aromatic system, thus adding to the stability of the ring torsion. MO 87 of the zwitterion and the dication do not possess electron density on the piperazine (see Figure 6.8; thus they shift density from the lone pairs of the carbon acid and the fluor atom to the aromatic system instead. However, in orbital 88 of the zwitterionic form, a small coefficient can be observed at the piperazine ring. Unlike the other protonation states, these two only involve orbital 87 and 88 for this absorption band.

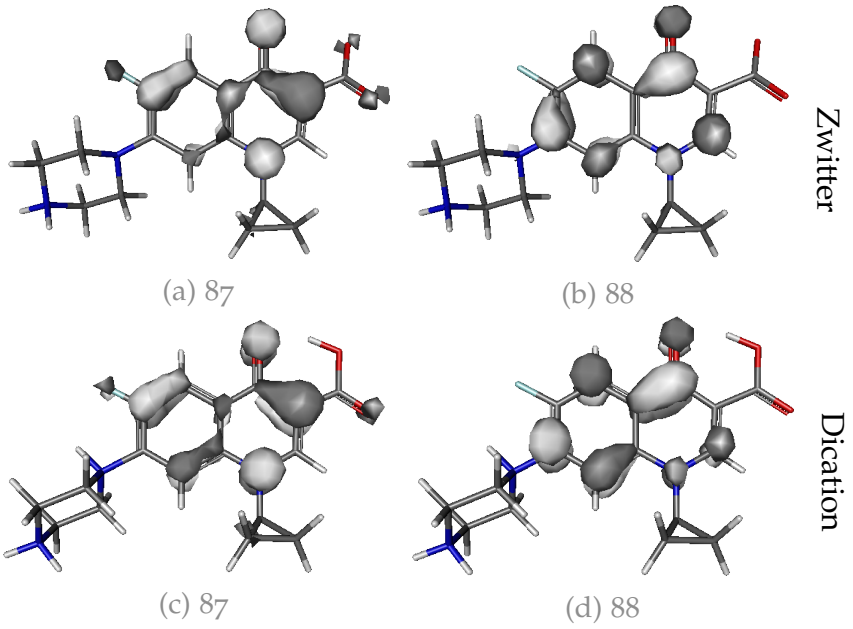

(a) 87 (b) 88

(c) 87 (d) 88

Figure 6.9: 1^{st} major transition: the MOs of the zwitterion and the dication

The second major absorption band is a $n - \pi*$ transition as well (Table 6.22. All compounds shift density from the piperazine group to the carbon acid, which is connected to the aromatic system - except the dication (see Figure 6.10).

Table 6.22: Comparison of the second major transition

Protonation State	Anion CIP^-		Neutral $CIPH$	Zwitter $CIPH$		Cation $CIPH_2^+$
Transition	S2	S3	S2	S2	S3	S2
nm	277.7	277.0	276.8	275.2	273.6	275.1
f	0.010	0.093	0.065	0.064	0.041	0.086
Prim. Orbitals	84->88	86->88	86->88	86->88	85->88	86->88
%	0.549	0.574	0.551	0.453	0.419	0.614
Sec. Orbitals	83->88	87->89	87->89	85->88	86->88	87->89
%	-0.232	-0.253	0.312	0.338	-0.364	0.288

The second major absorption band is a $n - \pi*$ transition as well (Table 6.22. Some

of the compounds possess two absorptions in a similar range; in such a case the absorption with the higher intensity was chosen. All compounds shift density from the piperazine group to the carbon acid, which is connected to the aromatic system - except the dication (see Figure

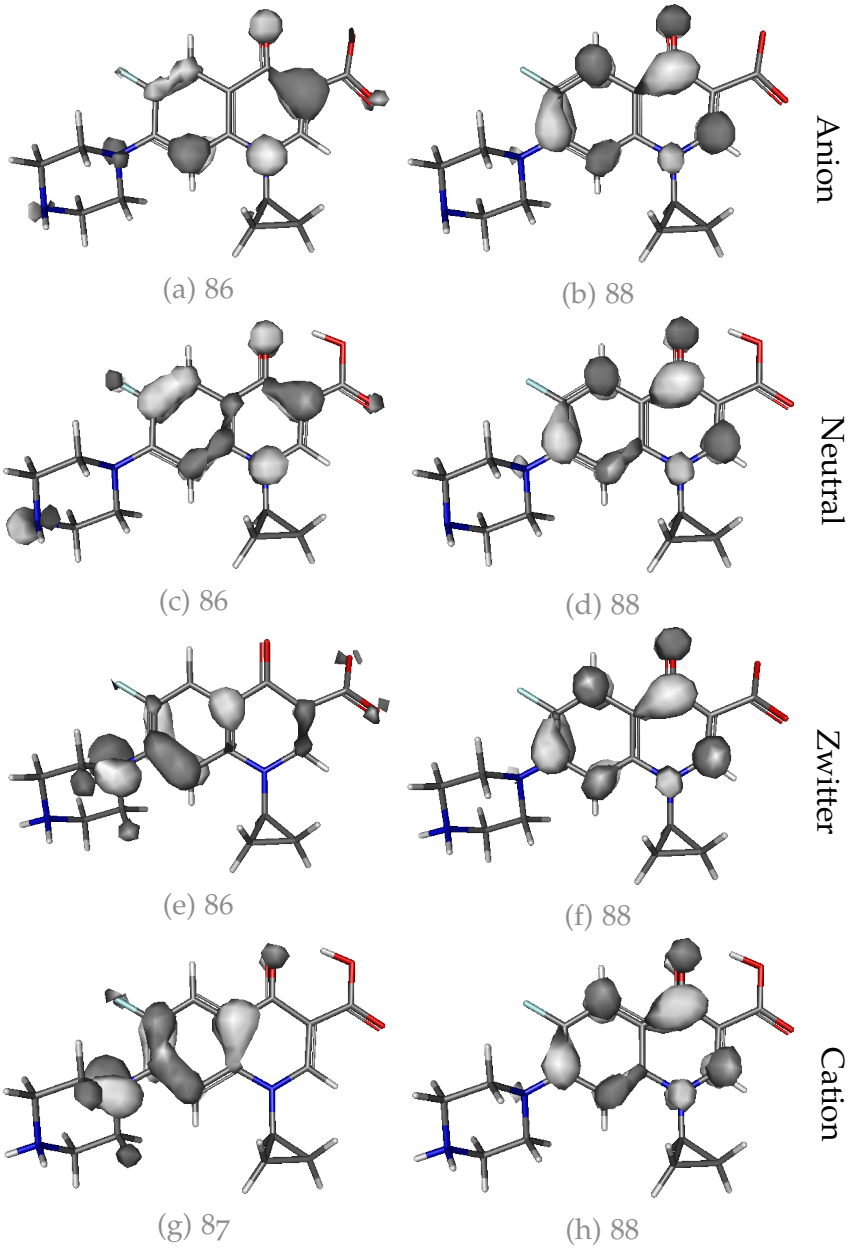

(a) 86 (b) 88

(c) 86 (d) 88

(e) 86 (f) 88

(g) 87 (h) 88

Figure 6.10: 2^{nd} major transition: the MOs of all forms except the dication

The dication lacks this transition due to the missing electron density on the piperazine moiety. For the anion, zwitterion and the cation the molecule orbitals of the number 86 are quite similar with respect to their coefficients at the piperazine, whereas the neutral form does not possess electron density at N'1, only at N'4. The cation also lacks electron density at the carbon acid group. All of the forms shown in Table 6.22 possess an additional transition from orbtial 87 to 89 - except the zwitterion, which uses orbital 85 and 88.

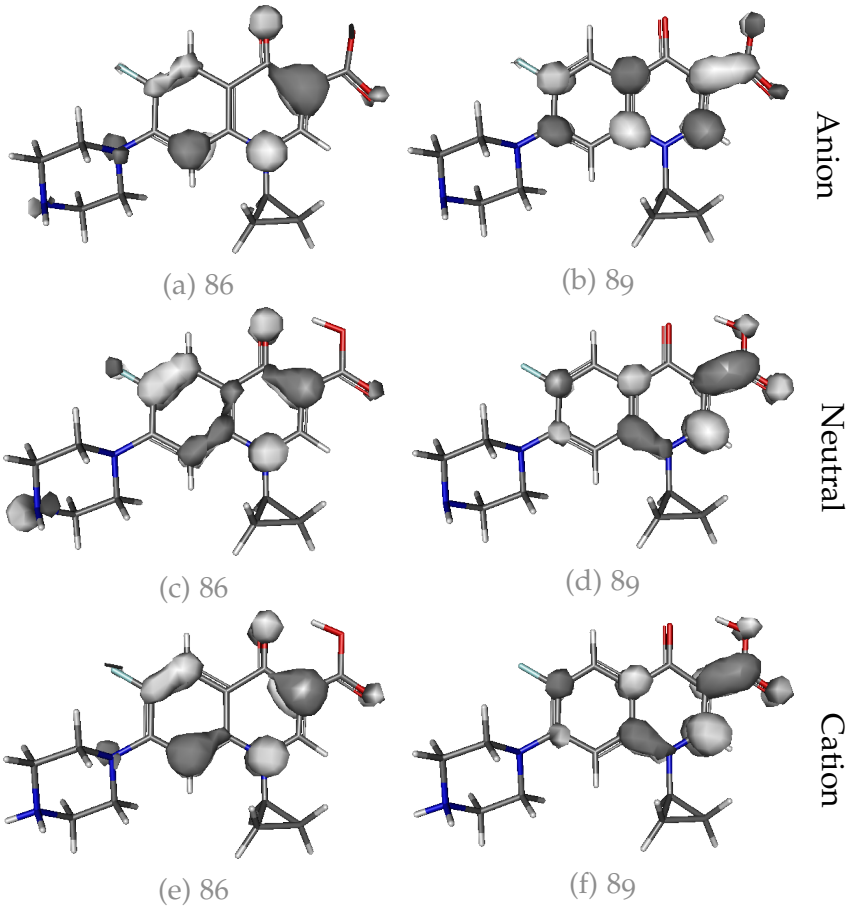

(a) 86 (b) 89

(c) 86 (d) 89

(e) 86 (f) 89

Figure 6.11: 3^{rd} major transition: the MOs of the anion, neutral and cation

The third transition takes electron density from the aromatic system close to the piperazine and shifts a part of it to the π-system of the carbon acid and its vicinity (see Fig. 6.11 and Tab. 6.23). It is thus a $\pi - \pi^*$ transition. For the anionic, neutral and cationic forms this includes the transfer of electron density from the piperazine to the aromatic system. These three protonation states also utilize orbitals 87 and 88 for a secondary transition.

Table 6.23: Comparison of the third major transition

Protonation State	Anion CIP^-	Neutral $CIPH$	Zwitter $CIPH$	Cation $CIPH_2^+$	Dication $CIPH_3^{2+}$
Transition	S4	S3	S4	S3	S2
nm	252.1	258.6	249.4	256.1	267.2
f	0.783	0.878	0.840	1.012	0.209
Prim. Orbitals	86->89	86->89	87->89	86->89	87->89
%	0.605	0.577	0.536	0.580	0.649
Sec. Orbitals	87->88	87->88	86->88	87->88	86->88
%	-0.251	0.252	0.325	0.326	-0.231

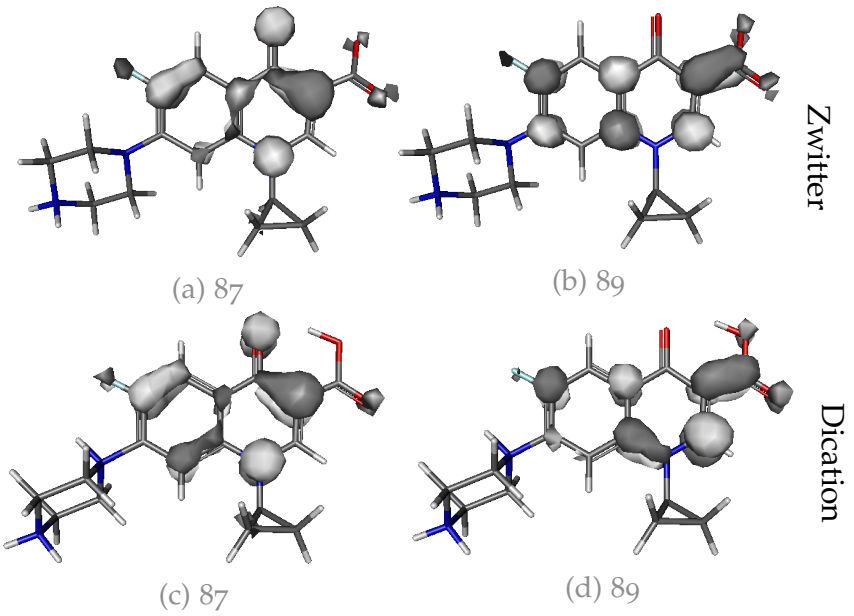

(a) 87 (b) 89

(c) 87 (d) 89

Figure 6.12: 3^{rd} major transition: the MOs of the zwitterion and the dication

The zwitterion and the dications primary absorption is analogue to those of the other protonation state, except for the lack of electron density on the piperazine ring (see Fig. 6.12) . Their secondary transition includes orbitals 86 and 89. The

absorption bands with the highest intensities mostly involve the orbital 86 to 89, both in primary and secondary transitions.

6.4 HOMO-LUMO Energies

Using the orbital energies from geometry optimizations of CIP with CAM-B3LYP/6-311+G(d) in water (SMD solvation), HOMO-LUMO gaps have been compared as depicted in Figure 6.13. This includes both ground and excited state (using the command TD(Nstates=8, Root = 1). The excited state of C1k is not included.

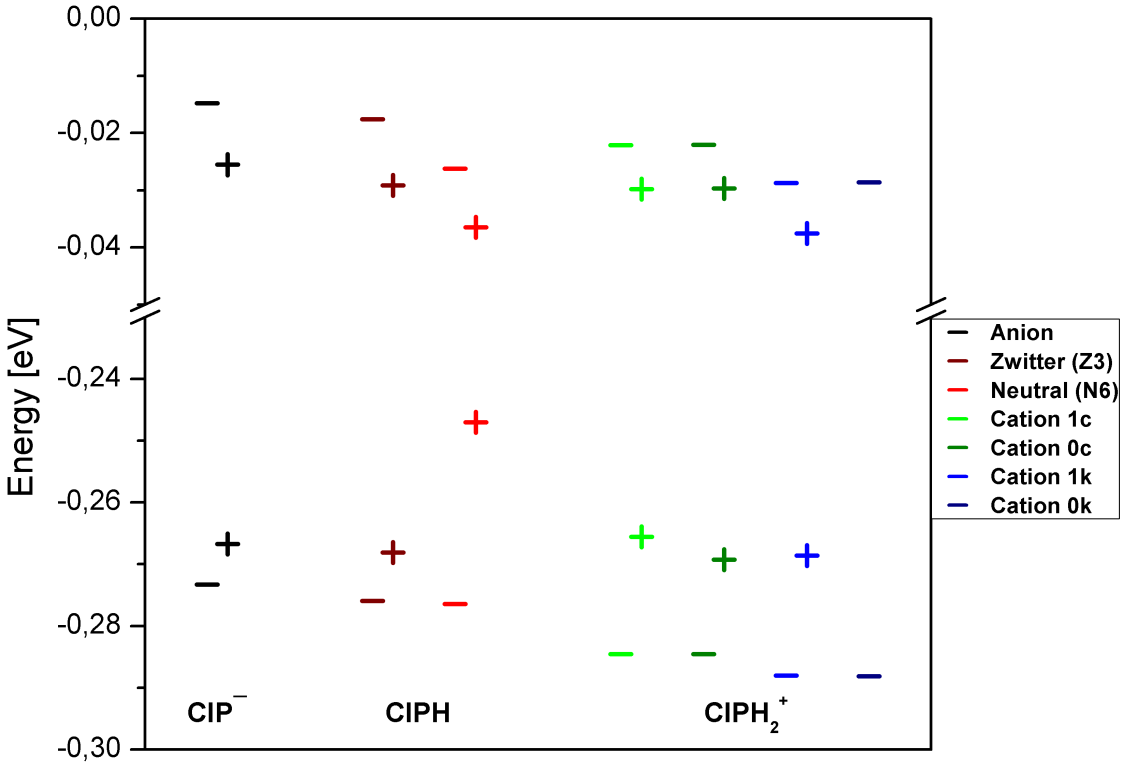

Figure 6.13: HOMO-LUMO gaps of energetically relevant protonation states of ciprofloxacin. Orbitals above the break are LUMOs, those below are HOMOs.'-' denotes the relaxed ground state, whereas '+' represents the the relaxed S1 state.

Excitation reduces the HOMO-LUMO gap among all compounds. On average, the highest occupied molecule orbitals are energetically more stable the higher

the positive charge of their respective molecule. This effect can also be observed for the LUMO in ground state. The gap between the HOMOs of the ground and excited state vary significantly among anionic and neutral molecules - in contrast, the cations show great consistency in this matter.

7 Conclusion

The aim of the work was the accurate theoretical prediction of the pK_a and UV absorptions of the fluoroquinolone ciprofloxacin (CIP), a pharmaceutically important molecule with various tautomeric forms. 2-naphthol (2N) and 4-nitrophenol (4NP) have been used for several tests to find a combination of density functional theory method, basis set and continuum solvation model which reliably fulfills these tasks. Several properties, conformers, tautomers and protonation states of CIP have been calculated with CAM-B3LYP/6-31++G(d)/SMD. From the computed results the following conclusions were drawn:

Continuum Solvent Models:
A preliminary test with 2N showed that SMD seems to be more accurate than PCM and CPCM and that the zero-point energy does not improve our pK_a calculations.

DFT-Methods:
Taking the excited state acid dissociation constant calculations (via Förster cycle) of both 2N and 4NP into account, the following trends can be observed:

- the corrected linear response (cLR) seems to overestimate the amount of the pK_a shift
- the state-specific approach is very inconsistent, some pK_a shifts differ by over 65 pK_a units between DFT functionals
- linear response (LR) seems to be very consistent with regard to the shifts, granted one chooses to use the absorption maxima
- employing emission wavelengths seems to perform in a less consistent manner than the same approach with absorption wavelengths

Considering the results of linear response paired with the absorption wavelengths, the DFT functionals APFD and CAM-B3LYP performed best. The ground state pK_a of 2N was best estimated by BMK and CAM-B3LYP. In the case of 4NP, which possesses a pK_a of 7.15, APFD and CAM-B3LYP showed the best estimations - however, they did underestimate it by roughly 2 units. CAM-B3LYP was thus chosen as main method for the ground and excited state pK_a calculations.

Regarding UV-Vis spectra, PBE0 showed the overall lowest error - however, the deviations were not systematic and their margin was greater than those of other methods. APFD performed quite similar, but with a lower range of errors. BMK, M06-2X and CAM-B3LYP consistently overestimate the energy of transitions. If the latter method is corrected by the values suggested by Jacquemin, it performs almost as well as APFD, but with very systematic errors. Overall, methods with low HF exchange appear to perform better with regard to electronic transitions. While both APFD and CAM-B3LYP are able to predict the trends shown in experiments to some extend, APFD is slightly better at it. Conclusively, it is the favoured method for this task.

Basis Sets:
The comparison of continuum solvent models with 2-naphthol showed that the aug-cc-pVTZ basis set is not suited well for the calculations of acid dissociation constants. On the other hand, for 2N the use of the Pople basis set 6-311+G(d) yielded results within less than 1 pK_a unit of the experiment - with the exception of APFD. Further tests with the Pople basis set showed that a second diffusion function only has minimal impact of the ground state pK_a. Adding a polarization function of the p-orbital type simply raises the pK_a by over 2 units - this yields similar results to the previously tested correlation-consistent basis set. This indicates that granting the hydrogen atom a p-orbital type polarization function might be inappropriate for pK_a calculations. Only the increase of basis functions consistently lead to improved results.

In view of the computation of absorption spectra, only a small difference was observed between def2-TZVP and 6-311+G(d): The former predicted the decrease in wavelength in the case of the second major transition, whereas the Pople basis set gives the same result for the anion and the zwitterion. Therefore, the preferred combination of method/basis set/solvent model is CAM-B3LYP/6-311+G(d)/SMD for pK_a calculation and APFD/def2-TZVP/SMD for the prediction of UV-Vis spectra.

Ciprofloxacin:
Calculations of several conformers of neutral ciprofloxacin resulted in a preferred neutral conformation (N6) and an almost equally stable zwitterionic conformer. The latter is equal to an experimental crystal structure named 'UHITOV', which can be found in the Cambridge Crystallographic Data Centre (CCDC).[47] With an RMS of 0.17 ± 0.11 eV, the absorption spectra calculated using APFD/def2-TZVP/SMD were in good agreement with the experimental spectra. The calculated protonation pathway is in line with the most recently published protonation scheme, which was proposed by Rusu and coworkers.[40] In this pathway, the neutral form can

be protonated either at the carbon acid moiety or at N4' (piperazine ring). The cation is protonated at both of the previously mentioned sites and the dication possesses an additional proton at N1' of the piperazine ring. While the preferred protonation was well predicted by our calculations, the pK_a values of the tri- and dication of CIP are too negative. The relaxed Born-Haber cycle seems to have difficulties not just with multiple positive charges, but also when both positive and negative charges are present: while the acid dissociation constants concerning the protonation/deprotonation of the neutral form of CIP are within 1.5 pK_a units of the experimental values, the zwitterionic form is predicted to be more acidic than the cation. In addition to the previously described problem, the unrelaxed Born-Haber cycle vastly underestimated the pK_a of the dication (-32.02 unrelaxed and -5.73 relaxed). The direct approach of calculating the pK_a yields similar and consistent results for both the neutral and zwitterionic form and overall performs slightly better than the Born-Haber cycle. Among the reaction schemes tested with CAM-B3LYP/6-31++G(d)/SMD, the simple dissociation reaction of the acid ($HA \rightarrow A^- + H^+$) yields the best results.

Fazit:
Protonation pathways are well predicted, but pK_a values of species with two or more positive charges are underestimated. In general, all our chosen DFT methods seem to require some improvement with regard to handling systems with multiple charges, assuming one does not want to use more than a triple-ζ basis set. The computation of excited state pK_as using linear response absorption wavelengths and the Förster cycle granted results within 2 pK_a units of the experimental value. We achieved the goal of the reliable prediction of UV-Vis spectra and trends among protonation states and are thus able to distinguish the compounds via UV-Vis spectroscopy.

8 Appendix

Experimental UV spectra at pH 2.02, 5.61, 7.64 and 12.53 shown in the left part of figure fig:ExpCIP were provided by our cooperators. [45]

Spectrophotometer:
PerkinElmer (Waltham, Massachusetts, USA) Lambda 20 Spectrophotometer.
Spectral range: 230-400 nm (1 nm) Slit: 2.0
Speed: 1920 nm min^{-1}

pH-Meter: Orion (Massachusetts, United States) 410 A potentiometer equipped with a Boeco (Hamburg, Germany) BA 17 combined glass electrode.
Anedra Calibration solutions pH 4.00, 7.00 and 10.00

Titration solutions: NaOH 5 mol L^{-1}, 1 mol L^{-1}, 0.1 mol L^{-1} HCl 37 %

Titration started with the addition of 70 μl of HCl 37 % to 50.0 ml of CIP 8.32 mg L^{-1} to reach pH = 1.91. Then, aliquots of NaOH at different concentrations were added to increment pH and the spectrum after each addition was measured until pH = 12.65.

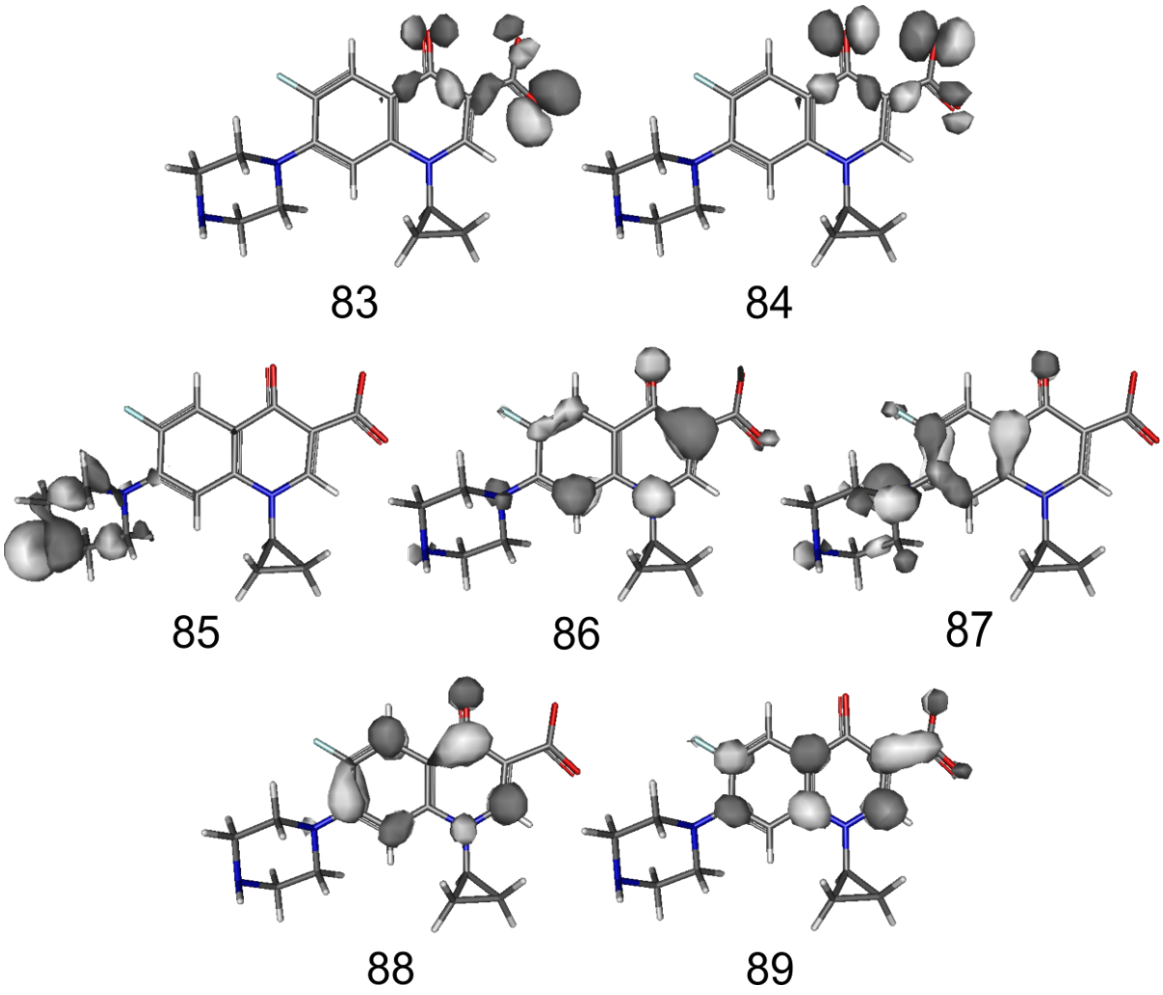

Figure 8.1: MOs of CIP^{-}. MOs 83-87 are occupied, 88 and 89 are unoccupied. Contour values of 0.05 a.U. were used.

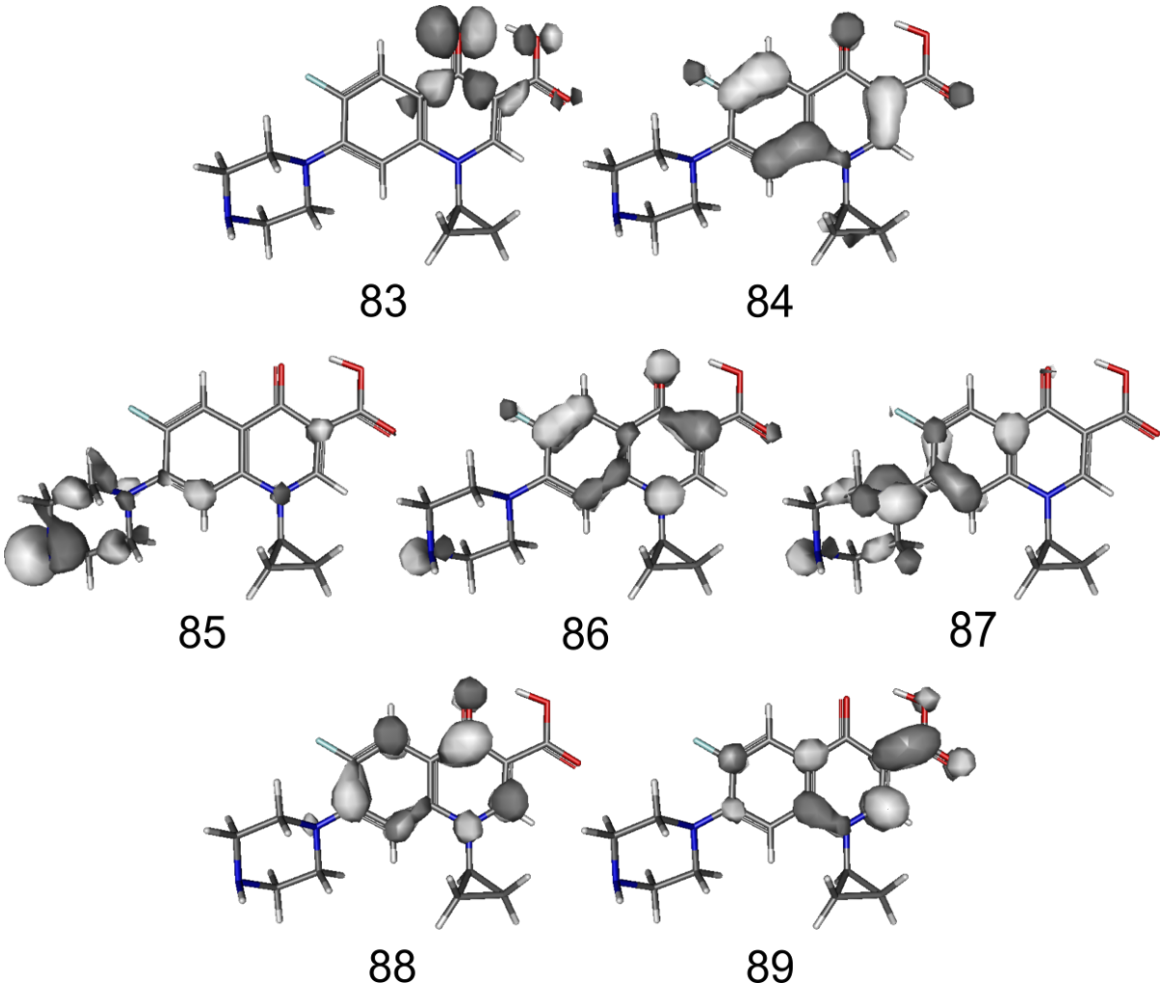

Figure 8.2: MOs of the neutral CIPH. MOs 83-87 are occupied, 88 and 89 are unoccupied. Contour values of 0.05 a.U. were used.

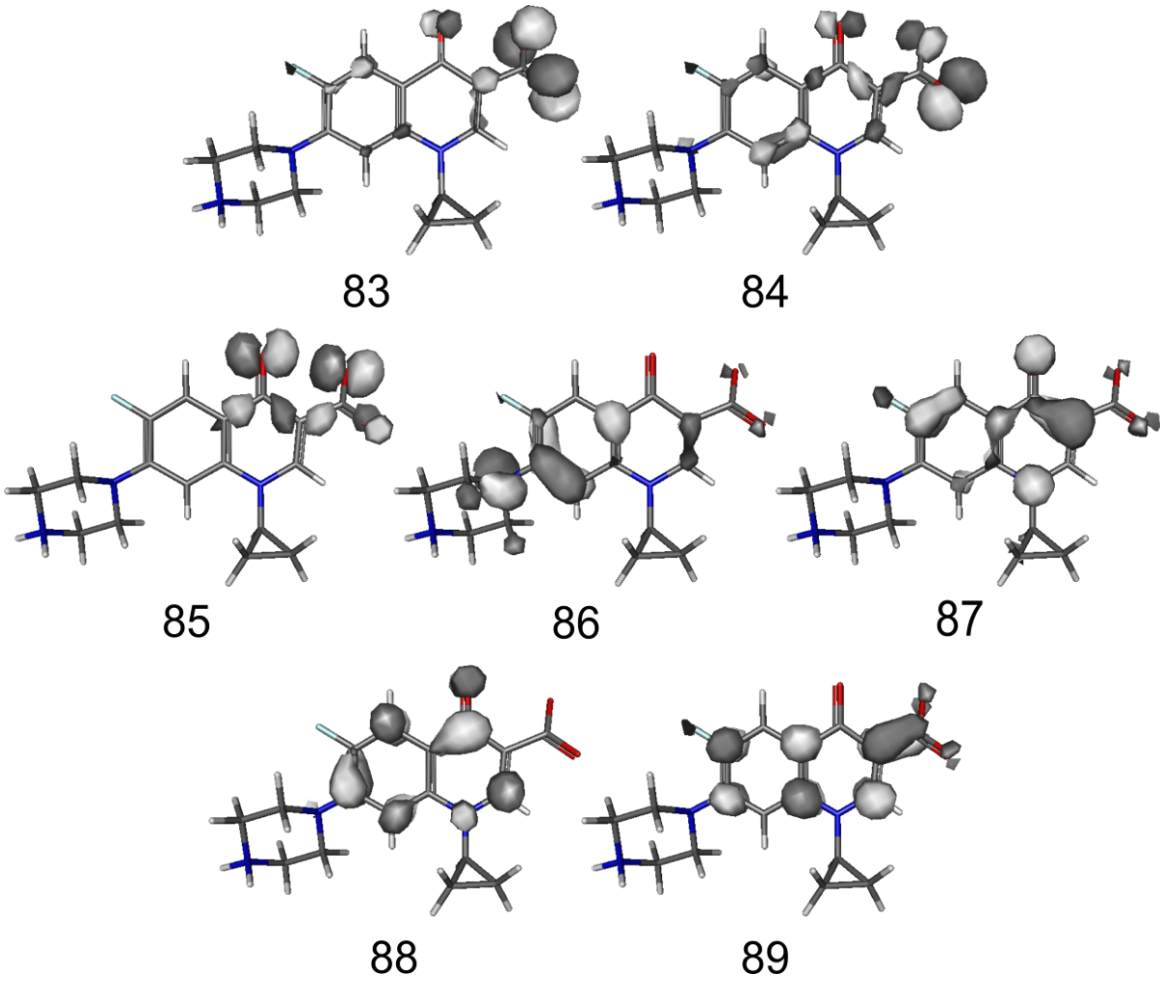

Figure 8.3: MOs of the zwitterionic CIPH. MOs 83-87 are occupied, 88 and 89 are unoccupied. Contour values of 0.05 a.U. were used.

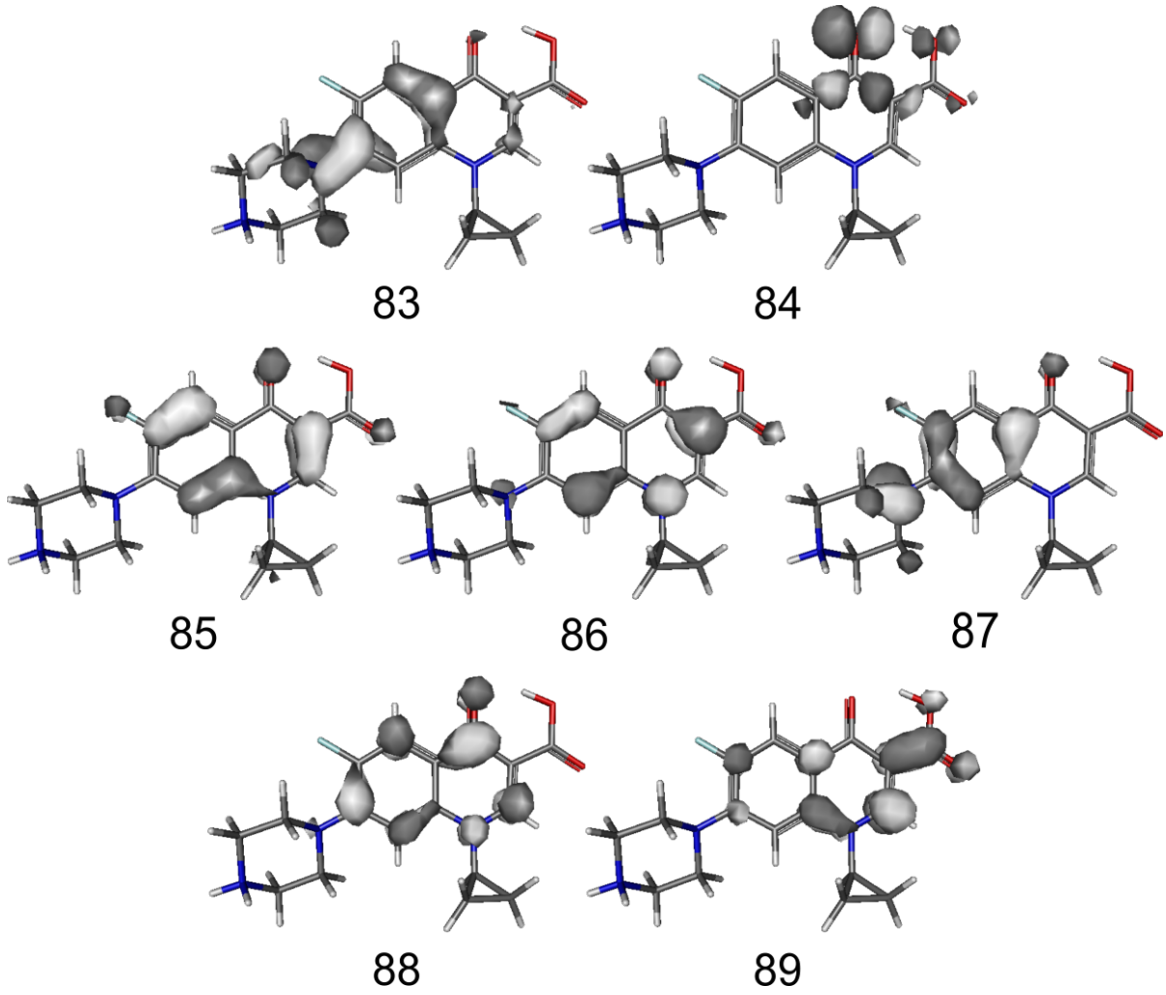

Figure 8.4: MOs of $CIPH_2^+$. MOs 83-87 are occupied, 88 and 89 are unoccupied. Contour values of 0.05 a.U. were used.

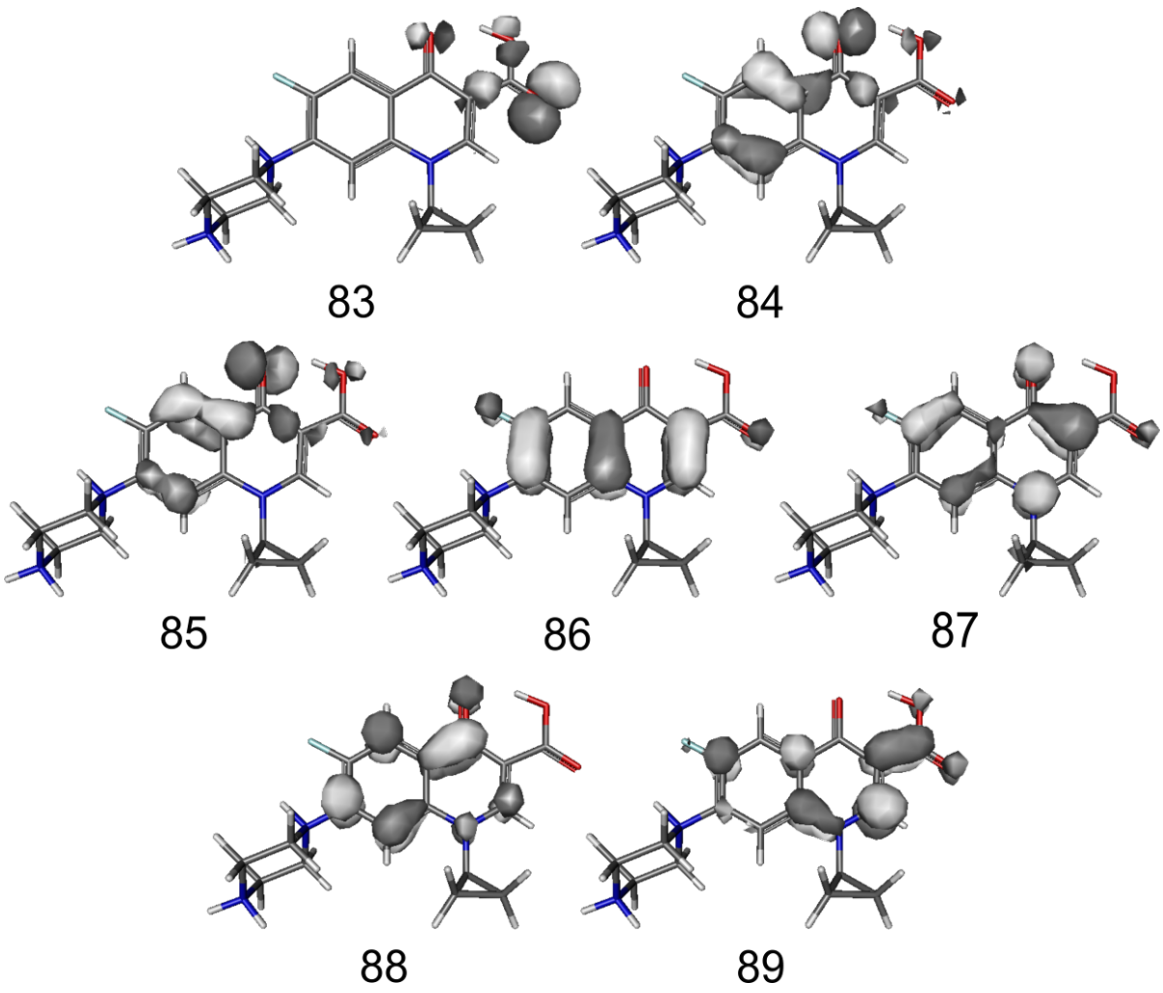

Figure 8.5: MOs of $ClPH_3^{2+}$. MOs 83-87 are occupied, 88 and 89 are unoccupied. Contour values of 0.05 a.U. were used.

Bibliography

[1] C. J. Cramer, *Essentials of Computational Chemistry: Theories and Models*, 2nd ed., John Wiley & Sons, Ltd, **2004**.

[2] Y. Houari, D. Jacquemin, A. D. Laurent, *Phys.Chem. Chem. Phys.* **2013**, *15*, 11875–11882.

[3] M. Isegawa, R. Peverati, D. G. Truhlar, *J. Chem. Phys.* **2012**, *137*, 1–17.

[4] C. Brückner, B. Engels, *J. Phys. Chem. A* **2015**, *119*, 12876–12891.

[5] A. Austin, G. A. Petersson, M. J. Frisch, F. J. Dobek, G. Scalmani, K. Throssell, *J. Chem. Theory Comput.* **2012**, *8*, 4989–5007.

[6] R. E. Stratmann, G. E. Scuseria, M. J. Frisch, *Chem. Phys. Lett.* **1996**, *257*, 213–223.

[7] A. D. Boese, J. M. L. Martin, *J. Chem. Phys.* **2004**, *121*, 3405–3416.

[8] A. D. Becke, *J. Chem. Phys.* **1997**, *107*, 8554–8560.

[9] T. Yanai, D. P. Tew, N. C. Handy, *Chem. Phys. Lett.* **2004**, *393*, 51–57.

[10] Y. Tawada, T. Tsuneda, S. Yanagisawa, T. Yanai, K. Hirao, *J. Chem. Phys.* **2004**, *120*, 8425–8433.

[11] Y. Zhao, D. G. Truhlar, *Theor. Chem. Account* **2008**, *120*, 215–240.

[12] Y. Zhao, N. E. Schultz, D. G. Truhlar, *J. Chem. Phys.* **2005**, *123*, 1–4.

[13] C. Adamo, V. Barone, *J. Chem. Phys.* **1999**, *110*, 6158–6170.

[14] T. H. D. Jr., *J. Chem. Phys.* **1989**, *90*, 1007–1023.

[15] F. Weigend, R. Ahlrichs, *Phys. Chem. Chem. Phys.* **2005**, *7*, 3297–3305.

[16] S. Miertus, E. Scrocco, J. Tomasi, *Chem. Phys.* **1997**, *55*, 117–129.

[17] V. Barone, M. Cossi, J. Tomasi, *J. Chem. Phys.* **1997**, *107*, 3210–3221.

[18] M. Cossi, N. Rega, G. Scalmani, V. Barone, *J. Comput. Chem.* **2003**, *24*, 669–681.

[19] A. K. Rappi, C. J. Casewit, K. S. Colwell, W. A. G. III, W. M. Skid, *J. Am. Chem. Soc.* **1992**, *114*, 10024–10039.

[20] A. V. Marenich, C. J. Cramer, D. G. Truhlar, *J. Phys. Chem. B* **2009**, *113*, 6378–6396.

[21] M. J. Frisch, G. W. Trucks, H. B. Schlegel, G. E. Scuseria, M. A. Robb, J. R. Cheeseman, G. Scalmani, V. Barone, G. A. Petersson, H. Nakatsuji, X. Li, M. Caricato, A. Marenich, J. Bloino, B. G. Janesko, R. Gomperts, B. Mennucci, H. P. Hratchian, J. V. Ortiz, A. F. Izmaylov, J. L. Sonnenberg, D. Williams-Young, F. Ding, F. Lipparini, F. Egidi, J. Goings, B. Peng, A. Petrone, T. Henderson, D. Ranasinghe, V. G. Zakrzewski, J. Gao, N. Rega, G. Zheng, W. Liang, M. Hada, M. Ehara, K. Toyota, R. Fukuda, J. Hasegawa, M. Ishida, T. Nakajima, Y. Honda, O. Kitao, H. Nakai, T. Vreven, K. Throssell, J. A. Montgomery, Jr., J. E. Peralta, F. Ogliaro, M. Bearpark, J. J. Heyd, E. Brothers, K. N. Kudin, V. N. Staroverov, T. Keith, R. Kobayashi, J. Normand, K. Raghavachari, A. Rendell, J. C. Burant, S. S. Iyengar, J. Tomasi, M. Cossi, J. M. Millam, M. Klene, C. Adamo, R. Cammi, J. W. Ochterski, R. L. Martin, K. Morokuma, O. Farkas, J. B. Foresman, D. J. Fox, Gaussian09 Revision A.02, Gaussian, Inc. and Wallingford CT, **2009**.

[22] R. Ditchfield, W. J. Hehre, J. A. Pople, *J. Chem. Phys.* **1971**, *54*, 724–728.

[23] M. Cossi, V. Barone, R. Cammi, J. Tomasi, *Chem. Phys. Lett.* **1996**, *255*, 327–335.

[24] M. Born, *Verh. Dtsch. Phys. Ges.* **1919**, *21*, 13–24.

[25] F. Haber, *Chem. Phys. Lett.* **1919**, *21*, 750–768.

[26] J. Ho, *Phys.Chem.Chem.Phys.* **2015**, *17*, 197–208.

[27] J. Ho, M. Z. Ertem, *J. Phys. Chem. B* **2016**, *120*, 1319–1329.

[28] J. Tomasi, B. Mennucci, R. Cammi, *Chem. Rev.* **2005**, *105*, 2999–3094.

[29] M. Caricato, B. Mennucci, J. Tomasi, F. Ingrosso, R. Cammi, S. Corni, G. Scalmani, *J. Chem. Phys.* **2006**, *124*, 124520–124533.

[30] R. Improta, V. Barone, F. Santoro, *Angew. Chem. Int. Ed.* **2007**, *46*, 405–408.

[31] Z. R. Grabowski, W. Rubaszewska, *J. Chem. Soc. Faraday Trans. 1* **1977**, *73*, 11–28.

[32] F. Neese, *Wiley interdisciplinary Reviews - Computational Molecular Science* **2012**, *2*, 73–78.

[33] A. R. Allouche, *J. Comput. Chem.* **2011**, *32*, 174–182.

[34] M. D. Liptak, G. C. Shields, *J. Am. Chem. Soc.* **2001**, *123*, 7314–7319.

[35] M. D. Tissandier, K. A. Cowen, W. Y. Feng, E. Gundlach, M. J. Cohen, A. D. Earhart, J. V. Coe, *J. Phys. Chem. A* **1998**, *102*, 9308–9308.

[36] D. M. Camaioni, C. A. Schwerdtfeger, *J. Phys. Chem. A* **2005**, *109*, 10795–10797.

[37] M. D. Liptak, G. C. Shields, *Int. J. Quantum Chem.* **2001**, *85*, 727–741.

[38] J. R. Pliego, J. M. Riveros, *Chem. Phys. Lett.* **2000**, *332*, 597–602.

[39] Z. R. Grabowski, A. Grabowska, *Z. Phys. Chem.* **1976**, *101*, 11–28.

[40] A. Rusu, G. Tóth, J. K. L. Szocs, M. Kraszni, Á. Gyéresi, B. Noszál, *J. Pharm. Biomed. Anal.* **2012**, *66*, 50–57.

[41] D. A. Buckingham, C. R. Clark, A. Nangia, *Aust. J. Chem.* **1990**, *43*, 301–309.

[42] Z. Qiang, C. Adams, *Water Res.* **2004**, *38*, 2874–2890.

[43] C.-E. Lin, Y. D. Jr., W.-S. Liao, S.-W. Sunb, W.-Y. Lin, C.-C. Chen, *J. Chrom. A* **2004**, *1051*, 283–290.

[44] A. V. Polishchuk, E. T. Karaseva, T. B. Emelina, V. E. Karasev, *J. Fluoresc.* **2012**, *22*, 373–379.

[45] M. Montemurro, *Laboratorio de Desarrollo Analitico y Quimiometria, Facultad de Bioquimica y Ciencias Biológicas, Universidad Nacional del Litoral, has thankfully agreed to use these data pre-publication*.

[46] D. Jacquemin, V.Wathelet, A. Perpete, C. Adamo, *J.Chem. Theory Comput.* **2009**, *5*, 2420–2435.

[47] C. R. Groom, I. J. Bruno, M. P. Lightfoot, S. C. Ward, *Acta Cryst. B* **2016**, *72*, 171–179.